Response inhibition in Premotor cortex corresponds to a complex reshuffle of the mesoscopic information network

Giampiero Bardella[2,3], Franco Giarrocco[1,2], Valentina Giuffrida[1,2], Emiliano Brunamonti[2], Pierpaolo Pani[2], and Stefano Ferraina[2,*]

[1]PhD Program in Behavioral Neuroscience, Sapienza University of Rome, Piazzale Aldo Moro 5, 00185, Rome, Italy
[2]Department of Physiology and Pharmacology, Sapienza University of Rome, Piazzale Aldo Moro 5, 00185, Rome, Italy
[3]INFN Sezione di Roma, Department of Physics, Sapienza University of Rome, Piazzale Aldo Moro 5, 00185, Rome, Italy
[*]corresponding author(s): Stefano Ferraina (stefano.ferraina@uniroma1.it)

ABSTRACT

Despite recent works have investigated functional and effective cortical networks in animal models, the dynamical information transfer among functional modules underneath cognitive control is still largely unknown. Here, we addressed the issue using Transfer Entropy and graph theory methods on neural activities recorded at the mesoscopic scale from a multielectrode array in the dorsal premotor cortex of rhesus monkeys. We focused our analysis on the decision time of a Stop-signal (countermanding) task looking for hallmarks in the network functional configuration, when the Stop signal is presented, that could influence the motor plan maturation. When comparing trials with successful inhibition to those with generated movement the nodes (modules) of the network resulted organized in four classes, hierarchically arranged, and differently partaking in information transfer. Interestingly, the hierarchies and the strength of the information exchanged between modules varied during the task, being different for generated movements and cancelled ones and coupled with distinct levels of network complexity and heterogeneity depending on the motor behaviors explored. Last, we exposed the multiscale structure of the network through the multi-fractal formalism, which allowed us to reveal the generating rules of the network and measure the distance between the information processed in the different behavioral conditions. Our results suggest that the premotor contribution to motor decisions involves a topological re-organization of the mesoscopic functional network whose intrinsic fractal features delineate its behavioral functionalities.

1 Introduction

The brain is a complex system formed by billions of neurons that, being densely interconnected give rise to networks organized in nodes (modules) of different dimensions. At the small-scale networks modules correspond to single neurons, at the large scale they are great-specialized brain areas. In between, at the mesoscale level, modules are aggregates of neurons (populations) of different sizes (e.g., functional columns and sub-populations). In the last fifty years, neuroscience has tried to describe brain computations by linking neural activities to behavior. Crucial in this process, at every scale of investigation, is the understanding of how different modules interact and how information is shared and processed among parts. In this context, the neurophysiological approach to brain functions with recording microelectrodes, performed mainly in animal models[1], provided invaluable advances. Indeed, the high spatial resolution of the method proved to be suitable in linking neurons activity to behavior, describing the organization

of local microcircuits and, sometimes, larger networks[2,3]. Most of these studies referred to the analysis of single unit activity, others focused more on mesoscopic signals as the local field potentials (LFPs), which indicates the average synaptic input to the explored area (for a review see[4]) and, to a lesser extent, on signals sampling the average spiking activity of discrete population (multiunit activity; MUA)[5–7]. Recent advances in microelectrode fabrication allowed us to locally sample, in the studied brain regions, sufficiently large populations of neurons and to approach the investigation of their collective dynamics. Indeed, it has been shown that neurons express more of their contribution to complex behavioral functions either when observed as coordinated functional ensembles[8–16] or described as common responses to the input they receive, supporting the modular organization proposed by pioneering studies[17]. In the motor domain, micro and mesoscopic descriptions (LFPs, MUA) have largely proved that the dorsal premotor (PMd) cortex of primates is linked to motor planning maturation and decision making[18–21]. However, except for the cosine population code introduced by Gergopoulos and colleagues about 40 years ago[22,23], most population-based descriptions have been proposed after the advent of the simultaneous multiple electrode recordings and mainly for single unit spiking activity. Here, we studied the PMd's local dynamics using the MUA obtained from single electrodes as a mesoscopic measure of spiking activity (SA, see Section 4.4) and implementing a combined information-theory and graph-theory approach to describe how the collective interaction of recorded modules (identified as the neurons producing collectively the measured SA) is linked to motor decision-making.

2 Results

The task the animals were engaged in (Fig.1) required either to move the arm toward a peripheral target (**Go trials** 75% for Monkey P and 68% for Monkey C) or to cancel the movement in case of appearance of a Stop signal (**Stop trials**; 25% for Monkey P and 32% for Monkey C). The two types of trials were randomly presented. During Go trials, after the disappearance of the central target (Go signal) the monkeys were instructed to reach the peripheral target to obtain the reward. In Stop trials, after the Go signal, the central target reappeared (Stop signal) after a variable delay, called SSD (Stop signal delay). In these trials the monkeys were required to refrain from moving to earn the reward (correct Stop trials). If the monkey were unable to stop, the trials were classified as wrong Stop trials, and no reward was provided. Since the SSDs were varied according to a staircase procedure based on the performance, correct Stop trials constituted approximately 50% of Stop trials (see Section 4.2 and Table 1). This task allows us to estimate the behavioral time window within which the decision to move (or to stop) is taken. The end of this interval, starting at the time of the Stop signal presentation, is commonly referred to as the Stop signal reaction time (SSRT). Table 1 shows the behavioral parameters of the 21 recording sessions analyzed in the present study (12 for monkey P; 9 for monkey C). Overall sessions, the average reaction time (RT) was 656 ms (129 ms SD, SD standard deviation) for Monkey P and 632 ms (119 ms SD) for Monkey C and the average SSRT was 217 ms (34 ms SD) for Monkey P and and 213 ms (26 ms SD) for Monkey C. Fig.2 shows, for one example session (S6) of Monkey P, the time evolution of the average SA obtained from each cortical module explored separately for Go trials (dark green traces), correct Stop trials (red traces) and wrong Stop trials (dark blue traces) in the time between the Go signal presentation and the end of the SSRT (see Figure caption for more details). For the session shown in Fig.2 we found that 76% of the cortical modules displayed a significant difference (ANOVA; $p < 0.01$) of activity between behavioral conditions after the Stop signal (vertical red line), i.e., during the session-specific SSRT. In the same interval, we found that 78% of the modules showed a significant difference between Go and correct Stop condition and 65% a significant difference between correct and wrong Stop condition (Bonferroni corrected for multiple comparisons). None of the modules showed significant difference between Go and wrong Stop condition.

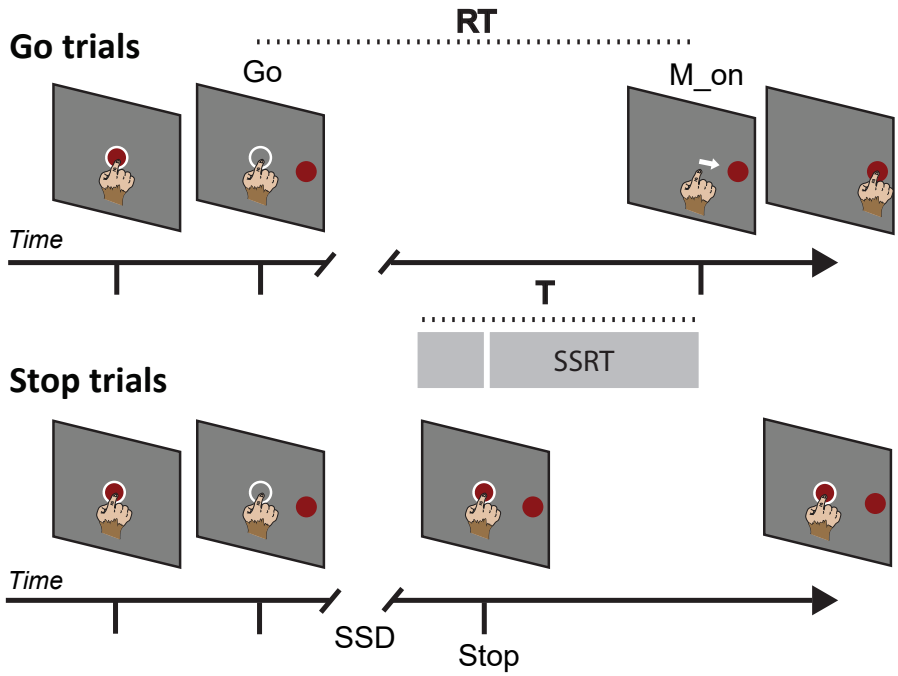

Figure 1. Sequence of behavioural events characterizing the task. Go and Stop trials were randomly intermixed during each session. The epoch (T) of neural analysis is shown as a grey bar for both trials. The duration of the epoch T was selected to always include the duration of the SSRT computed for each session. For further details, see Materials and Methods. RT, reaction time; SSD, Stop signal delay; SSRT, Stop signal reaction time. White circles are feedbacks for the touch provided to the animals. Go: time of Go signal appearance; Stop: time of Stop signal appearance. M_on: time for Movement onset.

Overall recording sessions (ses Table S1), there was a significant modulation of the SA sampled every 400 micrometers across the three behavioral conditions of the task, thus confirming previous observations on the involvement of PMd in inhibitory motor control and of the relevance of the epoch following the Stop signal appearance - in Stop trials - when decisions are taken[15,16,24–29]. However, at this stage, other than the heterogeneity of different modules in relation to the task, nothing could be inferred about the structure of the information transfer, the functional relationship between different modules , and the collective state of the network at the moment of the motor decision.

2.1 Information transfer in the PMd network is managed by hierarchically organized functional classes

To study the information transfer between the recorded PMd modules in the epoch in which the decision to perform/cancel the movement is taken, we used multivariate Transfer Entropy (TE), a well-established model-free information theoretic measure. To compute TE, we adopted a fixed epoch duration (T= 400 ms) among animals and recording sessions which allowed to include the estimated SSRT duration for each recording session as well as the last portion of the Stop Signal Delay - SSD - (see Fig.1, grey bar and Section 4.3 for further details). We then computed TE between the single-trial SA time series, in the epoch T, for Go, correct and wrong Stop trials. In a given epoch, TE can detect asymmetric information flow among modules allowing them to be classified as drivers (sources) or targets of information transfer (see Section 4.5 for details).

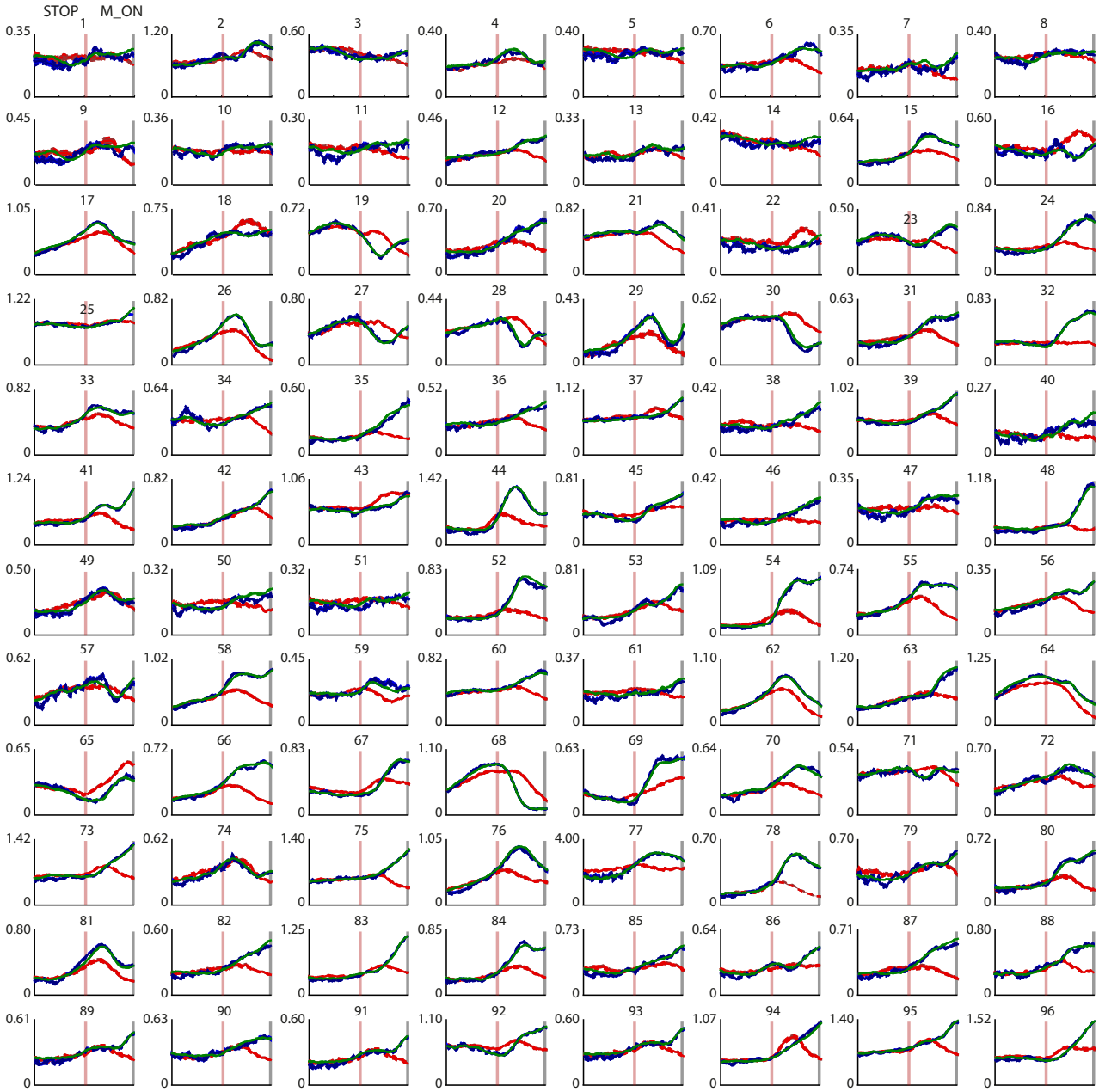

Figure 2. Heterogeneity of neuronal activity modulation in different trials type. Neuronal SAs (mean ± SEM) in the epoch T for the three behavioural conditions for all recording sites (modules) of S6 of Monkey P. Dark green traces show the average activity during Go trials aligned to Movement onset (gray vertical line). Dark blue traces show the average activity during wrong Stop trials aligned to Movement onset (gray vertical line). Red traces show the average activity during correct Stop trials aligned to the Stop signal presentation (light red vertical line) and plotted until the end of the SSRT. Each neuronal SAs is baseline corrected (see Section 4.4). For each plot the Y axes are units of SAs while the X axes mark the time during the epoch T; ticks in the first top left panel are every 100 ms. (**STOP**: Stop Signal appearance; **M_ON**: movement onset).

Behavioural Results							
Monkey P							
S	$\overline{RT}_{Go}$	$\overline{RT}_{Wr}$	$\overline{SSD}_{CS}$	$\overline{SSD}_{Wr}$	$SSRT$	$P_{inhibit}$	*p-value*
1	590 ms	559 ms	273 ms	337 ms	285 ms	0.52	$p < 0.05$
2	584 ms	565 ms	305 ms	408 ms	227 ms	0.50	$p < 0.05$
3	618 ms	592 ms	335 ms	430 ms	238 ms	0.52	$p < 0.05$
4	573 ms	549 ms	301 ms	401 ms	221 ms	0.50	$p < 0.01$
5	572 ms	540 ms	293 ms	379 ms	236 ms	0.50	$p < 0.05$
6	643 ms	625 ms	402 ms	496 ms	195 ms	0.51	$p < 0.05$
7	600 ms	568 ms	340 ms	441 ms	209 ms	0.49	$p < 0.01$
8	664 ms	641 ms	469 ms	525 ms	170 ms	0.57	$p < 0.01$
9	786 ms	753 ms	528 ms	627 ms	213 ms	0.55	$p < 0.01$
10	672 ms	619 ms	421 ms	500 ms	216 ms	0.57	$p < 0.01$
11	766 ms	721 ms	497 ms	504 ms	230 ms	0.51	$p < 0.01$
12	868 ms	853 ms	675 ms	746 ms	160 ms	0.55	$p < 0.05$
Monkey C							
1	598 ms	523 ms	322 ms	383 ms	250 ms	0.57	$p < 0.01$
2	539 ms	460 ms	382 ms	378 ms	158 ms	0.60	$p < 0.05$
3	561 ms	522 ms	318 ms	403 ms	207 ms	0.58	$p < 0.05$
4	672 ms	631 ms	423 ms	507 ms	217 ms	0.60	$p < 0.05$
5	638 ms	612 ms	401 ms	512 ms	189 ms	0.56	$p < 0.05$
6	579 ms	533 ms	308 ms	426 ms	224 ms	0.60	$p < 0.01$
7	667 ms	620 ms	383 ms	498 ms	240 ms	0.59	$p < 0.05$
8	697 ms	672 ms	430 ms	546 ms	223 ms	0.60	$p < 0.05$
9	688 ms	662 ms	401 ms	547 ms	230 ms	0.60	$p < 0.05$

Table 1. Behavioural results. S, index of the recording session. $\overline{RT}_{Go}$, mean reaction time of Go trials. $\overline{RT}_{Wr}$, mean reaction time of wrong Stop trials. $\overline{SSD}_{CS}$, mean SSD of Correct Stop trials. $\overline{SSD}_{Wr}$, mean SSD of Wrong Stop trials $SSRT$, Stop signal reaction time. $P_{inhibit}$, inhibition probability. The *p-values* result from the independence (Kolmogorov-Smirnov test with $p < 0.05$ between RT_{Go} and RT_{Wr} distributions).

Fig. 3 shows the TE matrix for each trial type obtained for the data in Fig. 2. A TE value > 0 indicates a statistically significant driver→ target relation for the pair of modules considered. As deducible from the dense horizontal stripes that vary between Go, correct and wrong Stop trials, a few of the modules are able to influence the activity of many others in the epoch where decision is taken, depending on the behavioral condition. To exhaustively describe the differences in the information transmission at the network level (i.e., the network topology), we resorted to graph-based measures. In this framework, each module is interpreted as a node of the network and each significant TE value as a link (or connection). We computed the vertex degree (VD), i.e. the number of connections per module, of the thresholded networks according to percolation analysis, thus removing the noisiest links[15,30–33] (see Section 4.6 for further details). A high VD score suggests that a module is functionally linked to many others. When VD is low the opposite is true. Furthermore, thanks to the asymmetry of TE, it is possible to establish, for each module, if information

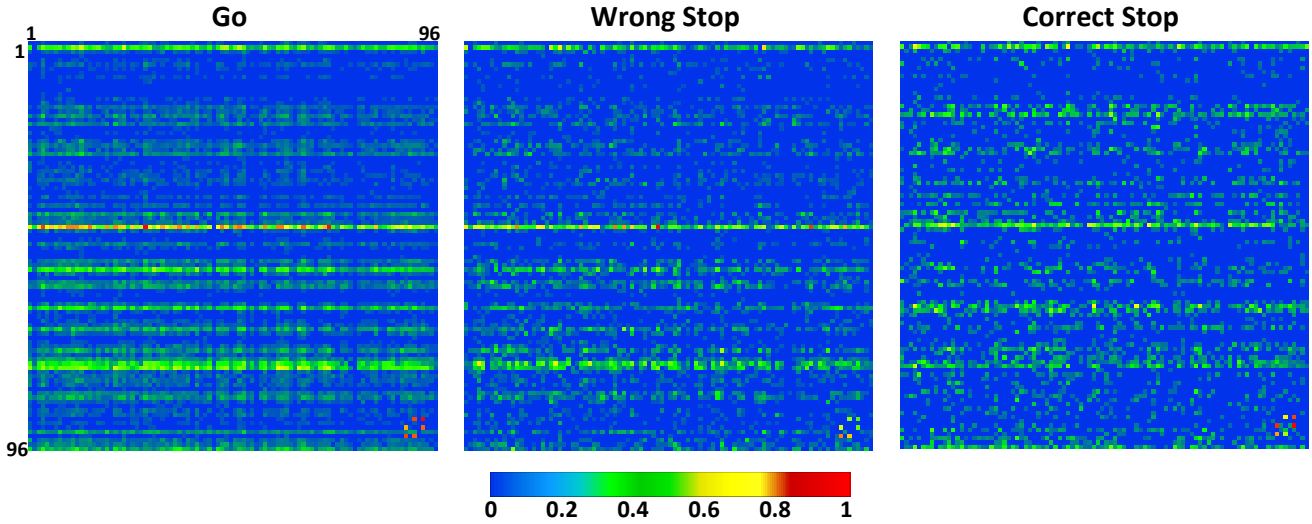

Figure 3. Average TE matrices of Go, wrong and correct Stop trials for data in Fig.2. Each entry of the matrix is color-coded according to the corresponding average TE value across trials. Statistically significant driver→ target relationships correspond to TE values > 0 for the pair of modules considered. Here, for graphical purposes, TE is normalized to the maximum across behavioural conditions so to obtain TE $\in [0, 1]$. The color bar indicates the normalized values of TE.

is directed to other modules (VD_{out}) or it is received from other modules (VD_{in}). We examined the VD_{out} and the VD_{in} distributions for each recording session of both monkeys and we observed, for all sessions and conditions, that only the VD_{out} distributions were fat-tailed (see supplementary Figure S1), hence suggesting the presence of modules with many outgoing connections compared to the average. These modules are referred to as network hubs[34–36] (see Section 4.6). This implies that the investigated information network had a more centralized organization when considering output connections than input ones. Using Go and correct Stop trials we then labeled the hubs according to the behavioral condition in which they emerged: some hubs were present in both trial types (**Super_drivers**); others only in the trials when the movement was generated (**Go_drivers**) or successfully canceled (**Stop_drivers**). All the remaining modules, never acting as hubs, were classified as **Neutrals**. Interestingly, when movements were erroneously performed following a Stop signal (wrong Stop trials), no new hubs were detected. This informs us that in trials in which errors occurs, the network handles information recruiting the same neural classes as Go and correct Stop trials (see also section 4.6). The percentage of nodes belonging to each class is shown in Table 2.

As briefly anticipated above, the direction of information flow identified by TE allow establishing a hierarchy of information transmission among modules. Indeed, according to the TE-based definition of drivers and targets, the past of a driver gives statistical significant contribution to the prediction of the present state of a target, putting the drivers hierarchically above the targets. To this extent, the emergence of network hubs pertaining to specific trial types (i.e., the classes) means that a few modules determine the state of many others, thus illustrating how the role of the classes is to selectively regulate the network's overall configuration depending on the motor behavior explored. At this point, one may wonder whether any internal hierarchy between classes exists, that is, whether the VD_{out} of the nodes belonging to a class selectively varies with the behavioral conditions. Thus, once the label of a node/module to a class was established according to the procedure explained above, the label was retained and how the VD_{out} of such nodes varied in different types of trials was studied. Through all sessions (see Table S2 and supplementary

Classes Composition	
Monkey P	$N = 96$
Class	$\boldsymbol{\mu \pm SEM}$
Go_drivers	9.3 ± 1.06
Stop_drivers	3.6 ± 1.4
Super_drivers	11.8 ± 1.6
Neutrals	71.3 ± 2.3
Monkey C	$N = 96$
Class	$\boldsymbol{\mu \pm SEM}$
Go_drivers	7.4 ± 0.8
Stop_drivers	4.1 ± 0.6
Super_drivers	9.4 ± 1.1
Neutrals	75.0 ± 1.8

Table 2. Classes composition. For each monkey the composition of classes averaged (mean ± SEM) over recording sessions is reported. N is the number of modules available.

Figure S2 for the single sessions), the Super_drivers had the highest values of VD_{out} compared to other classes in all three behavioral conditions, thus resulting as the primary information-spreaders hubs (Kruskal-Wallis, $p < 0.01$ Bonferroni corrected for multiple comparisons). Therefore, the Super_drivers are located at the highest hierarchical level in the network as they regulate information transfer whatever decision, moving or stopping, is taken. Conversely, the Go_drivers and the Stop_drivers displayed a different engagement (lower VD_{out} values) in Go and correct Stop trials respectively, suggesting that their hierarchical role changes in relation to the type of motor decision being processed. Indeed, the values of VD_{out} of the Stop_drivers were below the ones of the Go_drivers in Go trials and the values of VD_{out} of the Go_drivers were below the ones of the Stop_drivers during correct Stop trials. Interestingly, the Go_drivers had higher VD_{out} values during wrong Stop trials compared to correct Stop trials while the opposite holds for the Stop_drivers (Kruskal-Wallis, $p < 0.01$ Bonferroni corrected for multiple comparisons). This proves that, at the local level within the network, during wrong Stop trials a neural processing of information halfway between Go and correct Stop trials but more akin to that of Go trials unfolds. The presence of the four different classes of modules (3 different drivers and the Neutrals) straightforwardly show that the intrinsic composition of the PMd information network is heterogeneous, with some of the modules operating as driving hubs only in relation to a specific behavioral outcome (executing vs withholding the planned movement). In addition, the way in which the VD_{out} values of the classes vary across the trial types hints that the network configuration underlying information transmission is fine-grained and changes according to the decision leading to a specific behavioral output.

Fig. 4 illustrates the topology of the PMd network in the three behavioral conditions for data in Fig.3, highlighting the relevant features of the classes changing between conditions (Go_drivers and the Stop_drivers; for the networks including also the Super_drivers see Figure S2). Each link in the graph indicates the presence of a significant TE value between the corresponding modules (i.e. a non-zero entry in the TE matrix); the number of outgoing connections of each module reflects its VD_{out} value, i.e., the number of modules on which it acts as a driver. Modules are labeled (see Figure caption) according to the belonging class and links are coloured according to the source node they originate from. The centralized

organization of the information network is clearly visible in Go trials (and slightly in wrong Stop trials), confirming prior observations about the need for this functional state to facilitate movement generation[15]. It can be seen how, during wrong Stop trials, the same classes are active as in the Go trials. To this respect, Fig.4 (and supplementary Figures S3 and S4) show how the Go_drivers are hubs during Go and wrong Stop trials while the Stop_drivers emerge as important nodes of information spreading in correct Stop trials only. At the same time, it can be noted that the optimal centralized transmission present during Go trials is somewhat disturbed during Stop trials. This is evident from how, during the wrong and correct Stop trials, the link configuration is not "aligned" and "direct" as in the Go trials, but is apparently arranged following more steps and with a greater degree of complexity and heterogeneity.

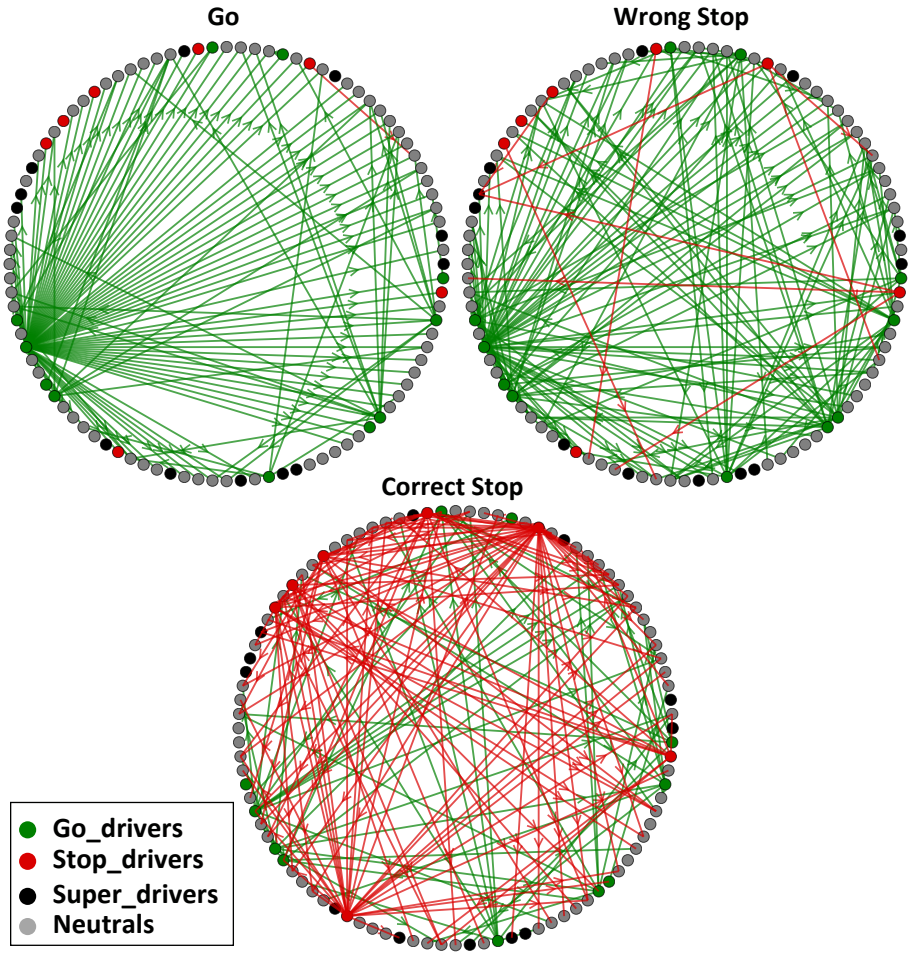

Figure 4. Partial information network of Go, wrong, and correct Stop trials. Data from the same recording session of Fig.2 and Fig.3. Each link is colour coded accordingly to the class its source node belongs to. Nodes with a high number of outgoing connections are the information-spreaders hubs (drivers; see legend in the figure). Here, for illustrative purposes and to better highlight the differences between behavioural conditions, the connections of the Super_drivers hubs are removed and for each network only the 20% of the strongest links are shown (for the complete version including the Super_drivers see supplementary Figure S3). The coordinates of each node on the circle are preserved across behavioral conditions.

Therefore, the emerging scenario is of a network preserving its constituent features (the presence of hubs) but changing in how these features are deployed - the classes and their different VD_{out} values - and organized - the emerging level of complexity - in relation to the needed behavioral control. In the following sections, we will formally quantify the topological details of the overall organization of the network (Section 2.2) and analyze how the hierarchical relations between classes shape the patterns of information spreading (Section 2.3). To conclude, we will explore, in section 2.4, the scale-dependent topology of the PMd information network, showing that it exhibits multifractal features. Such characteristics involve a set of underlying generating rules that link the intrinsic structure of the network to its functionality and make it possible to measure the structural distance between the information processed in the diverse behavioral conditions.

2.2 The organization of the PMd network shifts towards higher complexity in Stop trials

To characterize the global topological state of the network, we used percolation analysis. Percolation yields a curve in which the arrangement of the network structure is monitored as a function of the weights of the links (in our networks, TE). Usually, the measure used is the size of the giant component[37] or the number of connected components[30] (here we used the giant strongly connected component - GSCC - since the graph is directed; see Section 4.6). A stepped evolution of the curve testifies a non trivial hierarchical organization of the connections. Conversely, an abrupt and steep evolution, with no (or rare) steps, signals a random organization[15,30,37–39]. Moreover, the more a curve begins its descent to the right, the more complex the underlying organization (see also Section 4.6). Figure 5 shows, for all sessions, the results of percolation analysis compared between behavioral conditions and the null model (NM) for both animals. It is immediately noticeable (panel a) how the curves of the Go trials follow a different path than those of the Stop trials, with the former beginning its descent before the latter and having a more stepped trend. This is evidence, during Go trials, of the presence of fewer paths between nodes belonging to the giant component, with the majority of links with high information content pointing outwards to the rest of the network. This reveals an optimal network configuration in which communication is more direct than in the Stop trials. One implication is that the amount of redundant links is extremely small in Go trials, that is, there are few links that deviate from the overall organization. In other words, the majority of links with high weight are employed in a straight communication between the hubs and the rest of the network, thus lowering the level of complexity compared to that of the Stop trials. In the latter, on the other hand, the curves begin their descent further to the right (panel b), indicating a less optimal state than in the Go trials, with the presence of a higher number of low-length paths between nodes within the giant component. Hence, during Stop trials a complex rearrangement is in act, with denser communications and information with a high content that travels more within the component than outwards. Moreover, the proximity of the curves of the Stop trials to the curve of the null model (NM) reveals that, while they remain different from a purely random situation, they share some of its communication rules. Indeed, in the null model - which is complex by definition (see Section 4.6) - one expects a configuration whereby the links, being randomly arranged regardless of their weights, make the network dense with paths between nodes but with no stable configurations (as attested by the sudden descent without intermediate steps of the gray curve) and, most importantly, with no hubs (see also supplementary Figure S5). From the curve slopes (panel c), it can also be noted how the information required to reach comparable stable configurations (same values of y in Fig 5) is less in Go than in Stop trials, signaling that the higher intrinsic complexity of the latter is coupled with increased recruitment of resources. What has been said quantitatively confirms, at the global level, what was qualitatively grasped from Figure 4: namely, how local connections of specific classes shape the overall state of the network by altering its organization and affecting the pattern of information transmission in it. It also reinforces, at a deeper level given the measure used for link weights (i.e., TE),

the conclusions drawn in our previous work about the topological state that characterizes the generation and inhibition of a planned movement[15].

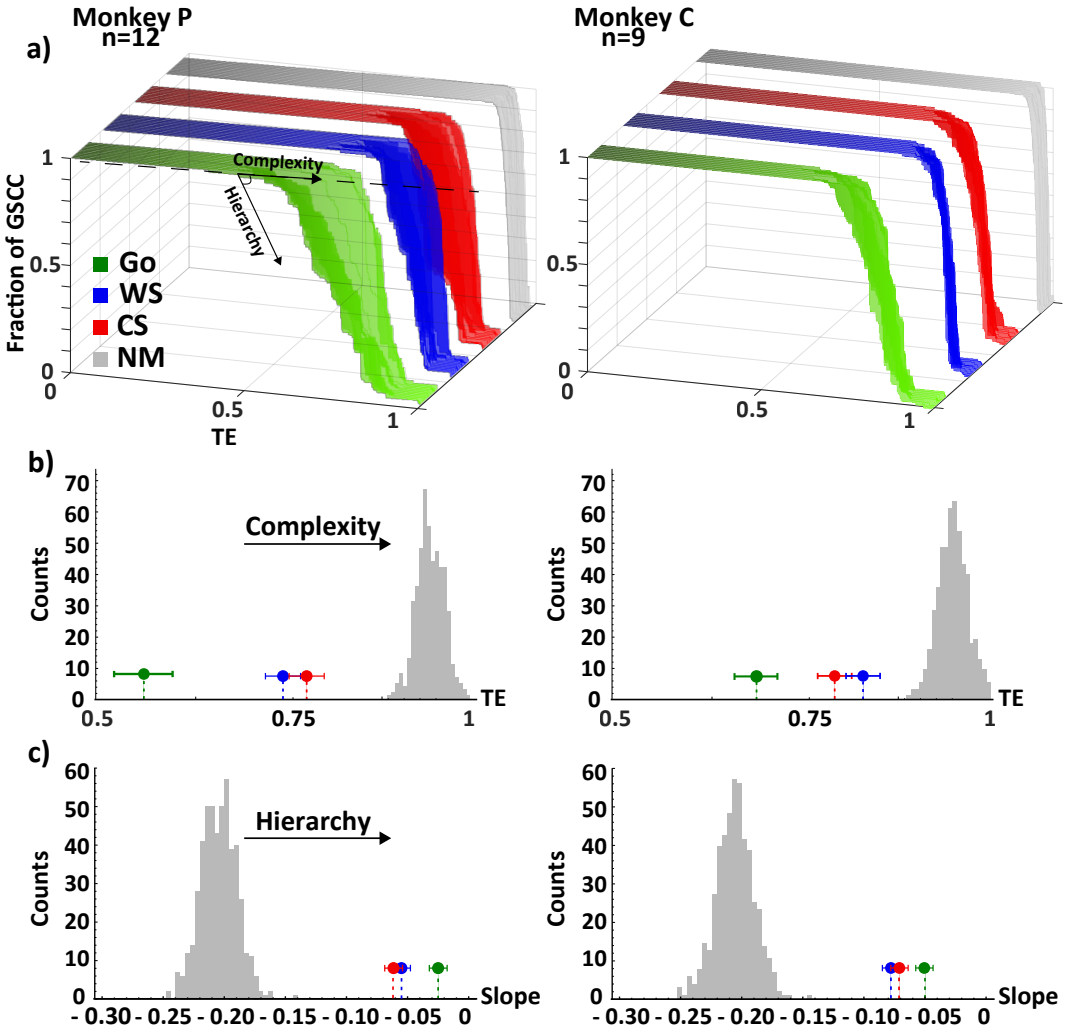

Figure 5. Percolation analysis. a: percolation curves over recording sessions compared across behavioural conditions and vs the null model for both animals. Each curve is a recording session. As sketched, the level of complexity of the underlying networks increases travelling the curves from left to right, whereas the hierarchy can be explored climbing down the steps of the curves (the fraction of GSCC, z axis), measured in unit of information (TE, x axis). **b:** comparison between the point of descent between behavioral conditions (mean $\pm$ SEM) and against the null model distribution. **c:** comparison between the measured slopes between behavioral conditions (mean $\pm$ SEM) and against the null model distribution. Stop trials resulted more complex and less hierarchical than Go trials (Kruskal-Wallis, $p < 0.01$ Bonferroni corrected for multiple comparisons) while having comparable values between themselves. In all panels, for simplicity and homogeneity, TE is reported normalized to its maximum so to obtain TE $\in [0, 1]$. The null distribution is obtained from 500 repetiztions of the null model (see Section 4.6.2). Since the null distributions for the different behavioral conditions were indistinguishable, we only reported one for brevity. (**GSCC**: Giant Strongly Connected Component; **Go**: Go trials; **WS**: wrong Stop trials; **CS**: correct Stop trials; **NM**: Null Model).

What has just been described, together with the mutual relationships among the VD_{out} of the classes reported in the previous paragraph, suggest that the contribution that each class brings to the overall network topology is different for each behavioral condition. Hence, to further clarify the hierarchical dependencies between classes and establish how the information managed by each of them is related to the overall organization of the network, we examined the VD_{out} as a function of TE, i.e., we monitored the evolution of VD_{out} of each class as a function of the percolation process. The procedure assesses the robustness of the information content of the links of each class relative to those of the rest of the network, thereby validating, globally and in a weighted manner, the hierarchical relationships measured through the VD_{out}. Indeed, for a class that is functionally relevant to a specific behavioral condition we expect not only a high number of connections (high VD_{out} value) but also for many of these connections to have a high and robust (high VD_{out} for high TE values) information content. This closes the loop, relating the local properties of the classes to the global state of the network during the three trial types. Results for the robustness analysis are reported in Fig. 6. As expected, the Super_drivers proved to be the class of highest hierarchical level in all three behavioral conditions. In fact, it showed the highest persistent values of VD_{out} as a function of the information processed. That is, it showed the highest number of links with high information content. Go_drivers and Stop_drivers then followed in this scale, confirming their complementary role in Go and in wrong Stop trials and in correct Stop trials respectively.

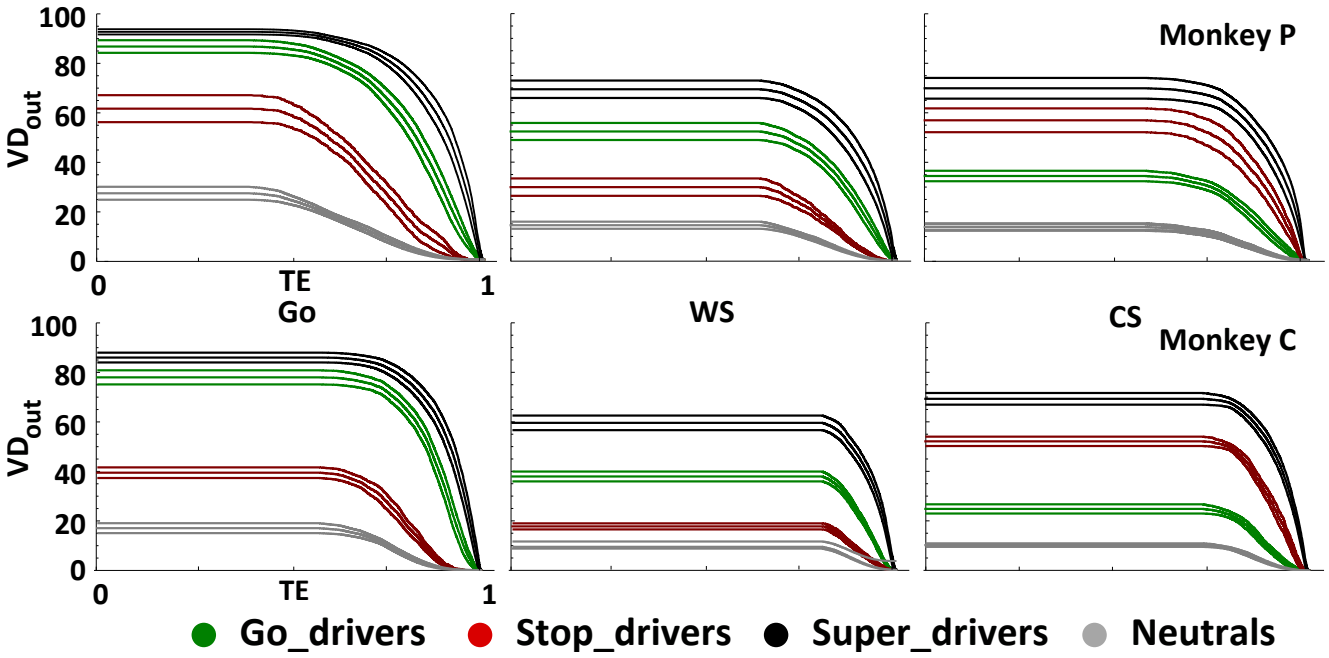

Figure 6. Classes robustness analysis. Robustness is inferred by monitoring the evolution of VD_{out} (y axis) as a function of the information processed (TE, x axis). Panels show the robustness curves averaged (mean $\pm$ SEM) over recording sessions compared between classes and across behavioural conditions. Curves are colour coded accordingly to the corresponding class as in Fig.4. (**Go**: Go trials; **WS**: wrong Stop trials; **CS**: correct Stop trials)

.

2.3 Distinctive interactions among neuronal classes characterize behavioural conditions

To summarize how the interactions between classes contributed in shaping the overall patterns of information transmission across behavioral conditions, we constructed an interaction **index I** proportional to the

strength of the information exchanged (see equation 5 in Materials and Methods). Through I, the all set of interactions between classes could be condensed in a 4x4 network representation in which each node is a class and the connections are the **I** values, that is, the weighted sum of the TE between the corresponding classes. This makes it possible to efficiently summarize in one number the hierarchical interactions between classes across behavioral conditions (see Table S3 and S4 for details). The Super_drivers were confirmed to be the highest order class in the network since they sent out the most information in all behavioral conditions compared to other classes. This implies that the Super_drivers determine the global state of the network, with the Go_drivers and the Stop_drivers playing a supporting role depending on the behavioral outcome. Indeed, the latter distributed the second highest information content in Go (and wrong Stop trials) and correct Stop trials respectively. In this regard, it is interesting to highlight how, in Go trials and wrong Stop trials the highest value of I, besides the one from the Super_drivers, was the one going from the Go_drivers to the Neutrals. In comparison, the contributions from the Go_drivers to the Stop_drivers and to the Super_drivers were negligible. The exact complementary situation was found in correct Stop trials, with the highest value of I, besides the one from the Super_drivers, detectable from the Stop_drivers to the Neutrals. It is worth noting that the direction and intensity of the interactions between Go and Stop drivers corroborated the specialization of such classes during behavioral conditions. Indeed, during correct Stop trials, information traveled from the Stop_drivers to the Go_drivers with an intensity an order of magnitude greater than it did in the reverse direction; the same applies to the flow from Go_drivers to Super drivers. Moreover, during Go and wrong Stop trials both contributions were comparably small and an order of magnitude weaker than during correct Stop. By combining these results with those obtained from the previous analyses, it is clear how the Go_drivers and the Stop_drivers are hierarchically at a lower level than the Super_drivers: not only do they express fewer connections but also the amount of influence they exert on other classes and their robustness is lower than that of the Super_drivers. The configuration observed during wrong Stop trials was, as expected, a hybrid between Go and correct Stop trials. On one hand it showed patterns of information transmission closer to the Go than to the correct Stop, of which the most notable were the highest contributions involving the Super_drivers and the Go_drivers, similar to those of Go trials; it also shared with the latter the negligible transfer between Go and Stop_drivers. On the other, it shared with correct Stop trials the same overall level of network complexity. To sum up, we have characterized the topology of the PMd information network by demonstrating the existence of different neural modules (classes) (Fig. 4) and how these classes distribute information differently (Table S2) contributing to the overall state of the mesoscopic network and its level of complexity, each with its distinctive intrinsic features (Fig. 5 and Fig. 6). All these aspects together define a hierarchy within the analyzed PMd network. We further refined the view of this hierarchy by diving into the details of how each class handled communications with the others depending on the behavioral condition, finding out that information is processed differently during correct Stop trials compared to Go trials and wrong Stop trials. Another interesting aspect emerged from our analysis: the nature of the Stop trials. Indeed, from what has been shown, it can be deduced that correct and wrong Stop trials share a topological organization that is similar in its overall features but differs in the details of how information is actually processed. Wrong Stop trials indeed showed a coexistence of interactions between classes comparable to those found in the Go trials and signatures of the attempted inhibition, as could be expected. Finally, results revealed the Super_drivers as the most topological central nodes in the network with the Go_drivers and the Stop_drivers playing a crucial supporting role in the processing of information during movement generation and inhibition respectively.

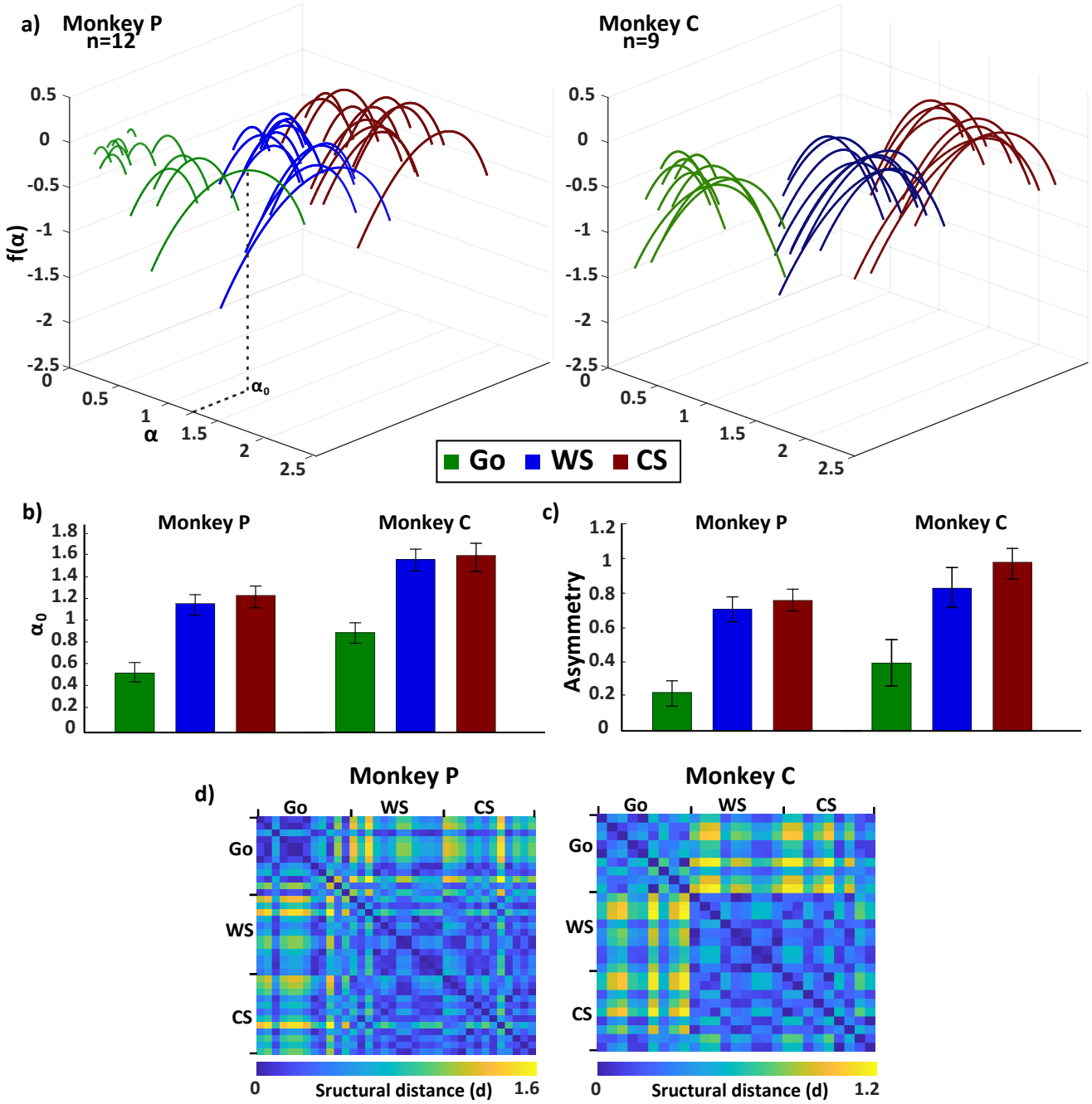

Figure 7. NMFA results. Metrics obtained from the NMFA framework compared across behavioural conditions for both animals. **a**: the multifractal spectrum $f(\alpha)$ compared over recording sessions for Go (dark green traces), correct (red traces) and wrong Stop trials (dark blue traces). **b**: the degree of structural complexity α_0 averaged over recording sessions for Go, correct and wrong Stop trials. **c**: the Asymmetry metric averaged over recording sessions for Go, correct and wrong Stop trials. **d**: pairwise structural distance matrix between behavioural conditions for all recording sessions. (**Go**: Go trials; **WS**: wrong Stop trials; **CS**: correct Stop trials)

2.4 A mutable multifractal arrangement of information transfer subtends motor decisions in the PMd network

To investigate the multiscale structure of the PMd information network across behavioral conditions and learn how its generating rules varied as a function of the motor behaviors explored, we resorted to the

multifractal formalism. More specifically, we used the recently introduced[40] node-based multifractal analysis (NMFA). The NMFA approach also provides a way to compute the structural distance between networks, which we employed to quantify the difference between the levels of information processed in the diverse trial types. Results of the NMFA are reported in Fig. 7. The NMFA distinguishes the fractal features of a network at different scales and quantifies its intrinsic level of complexity through a curve, called the multifractal spectrum, hereafter referred to as $f(\alpha)$. Panel a shows the $f(\alpha)$ over recording sessions for each behavioral condition and each animal. In $f(\alpha)$, the parameter α accounts for the level of complexity; therefore, $f(\alpha)$ describes how such complexity is distributed in the network. The degree of intrinsic complexity can be then easily expressed by a single number, α_0 (dashed black line in panel a, for one of the curves), that is defined as the abscissa corresponding to the maximum of $f(\alpha)$. The higher α_0 the more complex the network (see Section 4.6.1). Panel b shows α_0 averaged over the recording sessions for each behavioral condition and each animal. The values of $f(\alpha)$ and α_0 confirm that the PMd information network exhibits a more complex structure during Stop trials than during Go trials (Kruskal-Wallis: Monkey P: $p < 0.05$, Monkey C: $p < 0.01$). Significant insights into the topology and functionality of the PMd information network are further provided by the measure shown in panel c, the Asymmetry, which depends on the shape of $f(\alpha)$ (see Section 4.6.1). Asymmetry > 0 indicates a robust, efficient and stable mechanism of transmission, characteristic of the presence of hubs. Asymmetry < 0 indicates a more complex and heterogeneous and, to some extent, unstable transmission. Therefore, formal conclusions regarding the generating rules and functionality (here in the form of the mechanisms by which information is managed) of a network can be drawn based on the Asymmetry. In this regard, the results of panel c show that in our case Asymmetry was always > 0, indicating a consistent stability of the modality of information transmission across behavioral conditions, i. e. the one that employs hubs. This was to be expected, since we have thoroughly proven how the topology of the studied network possesses an internal hierarchy of nodes, that is, the one that gives rise to the classes. The reflections of this internal hierarchy are evident by considering the similar values assumed by the Asymmetry during correct and wrong Stops trials. Indeed, during Stop trials we saw how a condition-specific classes, quiescent during Go trials (low VD_{out} values, low robustness and smaller I contributions), i.e. the Stop_Drivers, emerge and re-route information in a different way than how it is processed during Go trials (Table S3 and S4). At the same time, we can deduce from Fig. 4, Fig. 5 and Fig. 6 how the topological backbone underlying information processing remains stable during Stop trials, however exhibiting a complementary role played by the Go_drivers in wrong Stop trials and the Stop_drivers in correct Stop trials respectively. Lastly, the ability to quantify the fractal dimension of network structures at various scales, made it possible to quantify the structural distance, d, between the information networks of the three behavioral conditions d is based on a mathematical transformation of $f(\alpha)$, i.e. the Lengendre transform (see Section 4.6.1). Given two networks, d efficiently encloses in one number the differences between their topological arrangements. We obtained a value of d for each pair of behavioral conditions for each session and each animal. The results are shown in panel d. d corroborates what has been shown so far: the overall topological organization occurring in the Go trials was far from that in the Stop trials, which were instead closer to each other. Therefore, on the one hand, NMFA provided us with insights into the structural scaling dependence of the topology of the network and a formal quantification of its fractal features. On the other, it allowed us to complement and further validate the conclusions, presented in the previous sections, about its complexity and heterogeneity by including them within a broader theoretical framework. In conclusion, what emerges from the results is that the PMd information network has a topological backbone with stable features that provides the common rules by which information is processed across behavioral conditions. Instead, the key difference between the motor behaviors explored is in the reshuffle of the actors involved, in their diverse hierarchical relationships, and in the different amounts of information processed.

3 Discussion

In this work, we investigated the patterns of local information transfer in a cortical network (the PMd) directly involved in movement decision-making. We used a combined Transfer Entropy and graph theory-based approach to analyze simultaneously recorded spiking activities (at the mesoscopic scale and from up to 96 channels). Our results contribute to moving forward the knowledge on the neural basis of motor control at different levels.

3.1 A topological approach to the organization and spreading of local information in a motor decision task

The first level of advancement is methodological: we employed a graph theory approach combined with information theoretic measures (specifically Transfer Entropy, TE) to investigate neuronal interactions underlying motor control. Although TE is growing in popularity in modern neuroscience, its application to invasive electrophysiological data has been so far very limited and restricted mostly to either single neurons or in vitro[41–44] and in silico studies[45]. Shimono and Beggs[41] used it at the single neuron level to investigate the structure at different scale of rodent somatosensory cortex[41,46]. Thivierge[44] used TE to examine the statistical dependencies between spontaneous neural activity recorded in cultures of cortical neurons. Timme and colleagues[47] recorded the activity of hundreds of neurons in cortico-hippocampal slice cultures and used TE to study the information transfer changes therein. An early contributions to this research topic is from Gerhard et al[48] that inspected the topology of spike trains recordings from the visual system of a rhesus monkey during a fixation task. However, the authors used a different approach to measure directed connectivity (the use of TE on invasive electrophysiological data from the visual system is also attributable to Besserve and collegues[49] which however did not resort to graph theory techniques). Another contribution comes from the work of Honey and colleagues, that investigated the relationship between the functional and structural properties of a large-scale interregional anatomical network of the macaque cortex through TE[50]. Here, both the spatial and the temporal scale of analysis were completely different considering that the authors simulated the time series of each brain region through nonlinear models of spontaneous neuronal activity. Wollstadt and collaborators also considered different (and larger) spatial and temporal scales than the one here presented[51]. Their work is of particular significance because it introduces for the first time a powerful method to estimate TE under nonstationary conditions, the so-called ensemble method (see Section 4.5 for further details). Such method exploits the multi-trial structure in neuroscience data to pool observation of neural activity over the ensemble of repeated trials instead of time, leading to a very accurate time-resolved TE. This represents a difference from the present work, where, instead, the exchange of information within the system is inferred in a fixed time window. Our choice was motivated by our interest to characterize the state of the PMd information network at a specific epoch of the task and compare it across behavioural conditions. To do so, we needed several network realizations in order to obtain a statistically robust estimate of its topological properties. In contrast, the ensemble approach would have led to a single representation of the temporal evolution of the network. A temporally precise but unique one. It could be argued that this constitutes a limitation of our analysis. Instead, we believe it is the way to answer a different scientific question. We also believe that the ensemble method is extremely powerful and plan to use it on our data in future studies. Lastly, an attempt to study voluntary action control through analysis of directed connectivity was made by Jahfari and colleagues[52] but on human MRI data. Hence, to the best of our knowledge, this report is one of the very few studies that use graph theory to analyze the information transfer network of a specific cortical area at the mesoscale level *in vivo* and during a behavioural task. The level of description here obtained is more detailed compared to previous works on motor control. Indeed, we were

able to specify how the decision on whether to move or to stop is implemented in PMd at the population level, who are the (key) players that manage information transmission, and how distant is the information processed across the different behavioral conditions. Notably, in our framework, neither any a priori assumption nor a specific neural modeling technique was needed. Our completely data-driven approach, in addition to complement the most recent models for the motor generation and suppression[53,54], permits us to overcome their main limitation which resides in the requirement of many biophysical parameters to be tweaked and tuned before fitting with acceptable accuracy the experimental data. In this regard, recently, more and more authors are applying graph theory tools to the study of neuronal interactions in different contexts and at different spatial scales. This provides great advantages in the case of inferential models that aim to estimate complex networks that represent functional and/or anatomical interactions between single neurons or entire brain areas[55,56]. It also proves particularly useful when one wants to directly analyze experimental brain networks and reconstruct their generative models[57,58]. For all these reasons, although is still not largely used in behavioural neurophysiological studies at the small and mesoscale, a graph theory-based conceptualization of neural interactions, possibly united with information theoretic measures, can be very profitable also compared to other common approaches relying on the analysis of covariance between neurons or mesoscopic signals[7,59–62] and should be exploited more. In fact, these methods are not straightforward in distinguishing the specific contributions of single neurons (or discrete populations of neurons) to the topology of network dynamics, which is our strategy's strength. On one hand, this range of methods allows for a fine temporal description of neural variability but on the other, due to their nature, are neither capable to describe the information flow between neuronal actors nor to provide quantitative insights on the topology of network connections and their hierarchical organization. Without this spectrum of details the computational strategy underlying motor control (and neural circuitry computation in general) would be yet elusive. Recently, some authors have started to follow the joint information theory-complex networks approach but for now, to the best of our knowledge, only on cortico-hippocampal[47], somatosensory cortex slice cultures[41] and during anesthesia[63]. It is known that to fully understand the neural mechanisms behind motor control future research should focus on cortico-cortical and cortico-subcortical interactions through massive simultaneous recordings. In this scenario, a topological information-based approach would be unquestionably necessary to gain an overall view and elicit detailed insights.

3.2 A race with more than two horses is in act in PMd when motor decisions are taken

The second level of advancement, which is closely related to the first, concerns the novelty of our results compared to other studies, especially those that focused on the possible interaction among different classes of neuronal assemblies during motor decision. We found, in the characterized PMd network, that neuronal activities could be organized around four different classes that actively participate, with different roles, i.e., through different topological attributes, both in movement execution and cancellation. This constitutes a step forward in the conceptualization of the neural processes that underlie movement generation since all the widely accepted models for inhibitory control of movements are deduced from the analysis of data from single electrodes recordings and are based on the interaction of only two modules (or class of neurons) often reported as Go and Stop units[53,54,64–67]. We instead demonstrated that information is hierarchically transferred between more than two actors, with the Super_drivers acting as the most important hubs for information spreading across behavioral conditions. This reflects the existence of an intrinsic high-order complexity in functional communications and organization at the population level, even in small portions of the cortex, during behavioural control, regardless of which the nature of neurons in each class might be (e.g., excitatory or inhibitory neurons). Indeed, based only on the information exchanged by each local module, we managed to isolate both condition-specific and nonspecific neuronal

classes. It is worth stressing that we drew our conclusion on the heterogeneity of neuronal classes in a completely data-driven and model-free fashion, and this strengthens the results. Additionally, we showed to what extent the information transfer within the network is linked to different behavioural outcomes and how the level of complexity and the patterns of information flows change between behavioral conditions. Our picture integrates the current view because besides specific classes more involved in the generation (Go_drivers) or inhibition (Stop_drivers) of movements, it establishes the existence of a high order class (Super_drivers) not proposed in other works. Based on the amount of information exchanged among the nodes forming the classes, we have been able to reconstruct the interaction patterns that characterize the inhibitory control of actions at the PMd level. These can be summarized by the diagram in Fig. 8. The Super_drivers are higher in the hierarchy with respect to the others for two reasons. The first is because they transmit the most information to the whole network than they receive from within it. Indeed, from the information-theoretic point of view, this means that the overall network state can be better predicted by the state of the Super_drivers compared to that of the other classes. At the same time, the state of the Super_drivers can be only minimally deciphered from that of the other classes. Thus, the configuration of the whole local network depends primarily on the Super_drivers. The second one is topological, being the Super_drivers the most important and robust hubs across behavioural conditions.

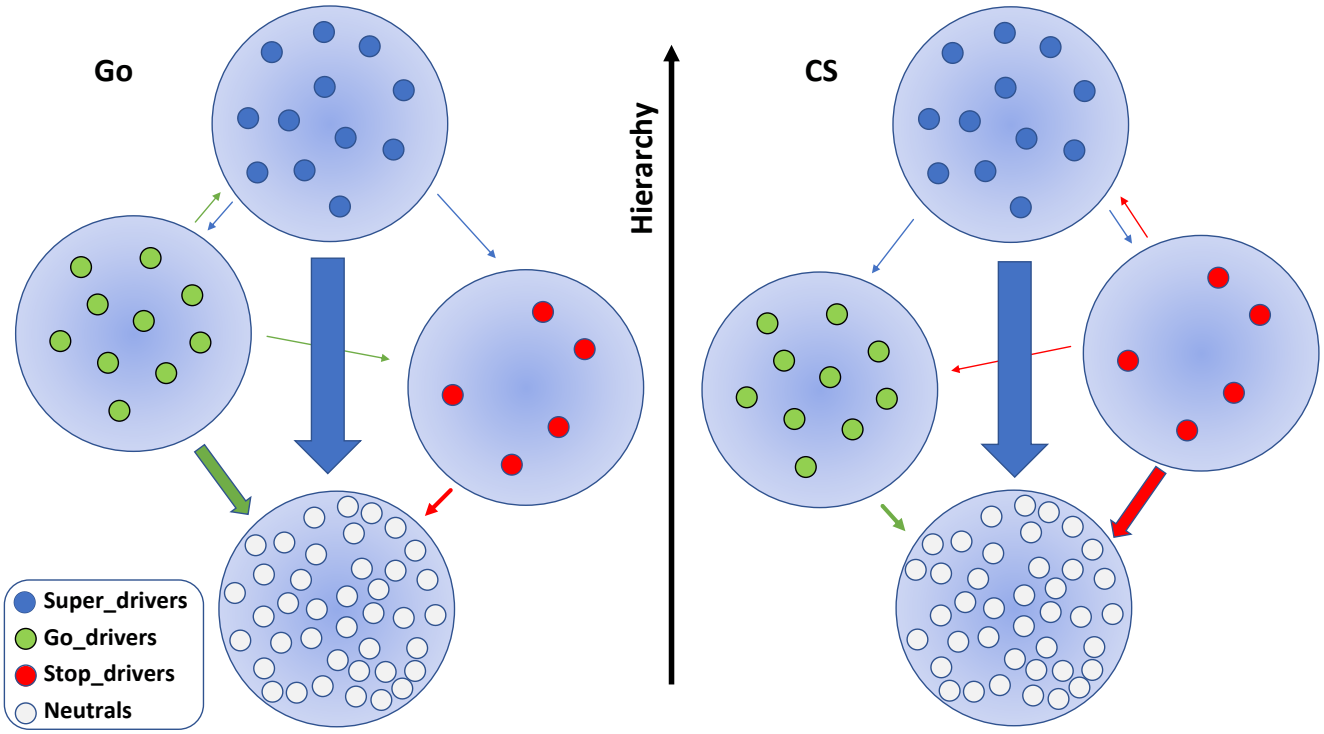

Figure 8. Information spreading among classes before movement generation and cancellation. Arrows between groups of modules are scaled according to the corresponding average (among sessions and animals) value of I. The level of hierarchy in which each class is ranked is graphically represented as the vertical positioning of the nodes; such level depends on the set of measures explored in this work and could be efficiently summarized by the index I. Since the Super_drivers is the dominant class in the network, its interactions are always shown. For the other classes, only the interactions at least one order of magnitude greater than the others and statistically significant across behavioral conditions are shown (see Tables S3 and S4 for further details).(**Go**: Go trials; **CS**: correct Stop trials).

Topologically speaking, the degree of formalization that percolation and multifractal analysis allow, significantly increases the breadth of theorization about the processes underlying motor control that we attempted to give in this study. Indeed, they enabled us, through their formalism rooted in statistical physics, to describe in great detail the topological structure of the analyzed PMd network, revealing higher-order connectivity patterns and relating its structure to the functionality performed during the task. In our case, the bridge between structure and functionality is markedly pronounced since the links in our network represent the amount of information exchanged between neuronal ensembles within the PMd.

Regarding the behavioral functionality, according to the race model, the Stop process should be 'activated' only in the Stop trials following the presentation of the Stop signal. However, increasing evidence[68,69] suggests that the Stop process is also active in Go trials. Our results show, at least in the context of information exchange within the PMd, that such co-activation corresponds to a network organized in four classes of information modules. This is matched by the different hierarchical levels in which the Go_drivers and Stop_drivers are ranked in the different behavioral conditions. Moreover, our results also show that the Stop_drivers exhibit a flow of information directed to the Super_drivers that is significantly higher during correct Stop trials compared to the other behavioral conditions. This suggests that some of the information that the Stop_drivers handle in attempting to abort the movement is directed to influence the Super_drivers, which are extensively involved in facilitating the overall process. Considering all its aspects, the pattern of information transmission in the network suggests that the reason why the attempt fails in the wrong Stop trials is related to the strong flow directed from the Go_drivers to the Neutrals, as it occurs in the Go trials and to the limited involvement of the Stop_drivers, which distribute considerably less information than in the case of properly inhibited movements (see also Table S3). This highlights, for the first time at the mesoscale resolution, the existence of a fine-grained organization of neural assemblies at the population level that handle intra-area information flow. It is worth pointing out that usual methods of studying neural activity profiles are not sufficient to infer all aspects of such architecture. The found subdivision in classes, the presence of hubs, i.e. topological central nodes deputed to sort out the communications, reveal that the cortical information dynamics behind motor control is extremely rich and cannot be entirely explained by the current proposed models. The topological organization we portrayed also implies that the presence of high-degree nodes is a constituent feature of neural processing in a cortical network directly involved in cognitive control, as is the PMd. This is reinforced by the finding that the topological structure detected across behavioral conditions exhibits stable rules for the information transmission system: the one based on hubs. This is consistent with our previous study[15], in which we showed how the functional PMd network organization differs between movement generation and inhibition in terms of hierarchy and centrality of nodes. It is also in agreement with other works that found fat-tailed degree distributions in silico[70], in cortical and hippocampal in vitro networks[41,71–74], in vivo[75] and anatomical structural networks[50]. Within this topology, different information exchange regimes realize, which are reflected in specific quantifiable differences. On one hand correct and wrong Stop trials resulted to have similar levels of complexity. On the other, during Go and wrong Stop trials classes were recruited to exchange information in a similar fashion. This attests that the peculiarities of the arrangement of the PMd information network depend on the outcome of the motor behavior, passing from a purely centralized state during Go trials to a different one during Stop trials, the latter characterized by an higher level of complexity, an increased degree of randomness and a different scheme of information transfer. This change is of particular interest because it signals a strong association between the mode of communication between nodes and the specific behavioral condition. Most notably, the structure found in the Go trials implies a high and very robust communication strategy compared to that observed in trials in which a Stop is presented. Considering also the results from our previous study[15], this thus appears to be the preferred mode of information transmission, at the PMd level, when a

movement is planned and then executed. Similarly, the network state to be associated with a planned and then inhibited movement seems to correspond to one that is topologically very similar to the previous one but in which some degree of randomness is, however, "injected" into the interactions. What demonstrated in the present work adds a very important piece to the puzzle, that of the fine-grained, yet flexible, fractal hierarchical organization realized through the classes. All this gives us an insight into how a network involved in a cognitive task is capable of changing the goal of its functionality by changing its degree of complexity and heterogeneity at different scales, recruiting different resources but keeping the generating rules of its topology stable. In particular, we interpret the reorganization occurring in correct Stop trials as the execution in the local network, through the intervention of the Stop_drivers, of a command originating from other regions. Indeed, as known, the PMd is part of a larger network surbserving motor control based on frontal, parietal, subcortical and spinal structures. It is reasonable to think that during Go trials the hubs serve to convey the command to move to other (and possibly anatomically lower) cortical, subcortical, and spinal circuits that will eventually promote muscle activation. In this picture, the state observed during correct Stop trials could reflect the PMd collective reaction, to the incoming inhibitory input that prevents the execution of the programmed movement. Therefore, the volition to inhibit would be locally implemented as 'the attenuation of the movement state', that would be obtained by tuning the level of randomness in the wiring scheme of the network with a resulting more complex organization. This seems convenient ad easy to implement at the level of network dynamics in that it would be sufficient, in order to spread the message, to recruit dedicated resources (the Stop_drivers) and to detour the information flow through different paths between nodes. Along these lines, the state recorded during a wrong Stop, being topologically relatable to that of a correct Stop and, at the same time, showing the same patterns of information transfer of Go trials, would result from an erroneous transmission of the inhibitory coding, probably due to a persistent strong recruitment of the Go_drivers and a contemporary weaker involvement of the Stop_drivers, as it happens during Go trials. This is in agreement with what we described in one of our recent papers in which we analyzed the dynamics of neural activity in the same task with a state-space approach[29]. Indeed, in such a scenario, we demonstrated how a subspace in which neural activities are confined before movement generation and during movement suppression exists.

One weakness of this study is that we cannot account for the information dynamics between PMd and other structures of the reaching network. Therefore, additional research, in a multi-area framework, will be needed to unambiguously clarify the interactions of the PMd network with other structures and to investigate to whom the hubs project or are connected to. Also, considering the nature of the mesoscopic signal studied, it was not possible to resolve the contributions of individual neurons within each of the modules forming the classes. In order to do so, one can consider extending the approach presented in this study to the analysis of the activity of individual neurons as well. Lo et al.[54] also introduced a certain degree of hierarchical organization in the form of a top-down control regulating the activation of the Go and Stop units. However, as also stated in Schall et al.[66], the control unit embodied in their model resembled an external homunculs endowed with the ability to tune the parameters to appropriately obtain the desired results. This marks a considerable difference with our report, in which, since our approach is completely data-driven, we did not need to adjust any external modelling unit to obtain the results. Conversely, we used it conceptually to contextualize our results in a wider circuitry frame. Lastly, our findings clearly show that hierarchical control is not only external but is also implemented locally by a specific neuronal class (the Super_drivers) over the others. Throughout the years, much evidence has been brought to support the idea that the brain is hierarchically organized both globally and locally on a spatial[15,30,76–86] (for a detailed review see Hilgetag et al., 2020[87]) and temporal scale[88–93]. As far as we know, this is the first work that deeply investigates the local topology of a single cortical area known to have a crucial role in the motor system. These conclusions suggest that the collective network organization

found in this work represents the neural implementation for the voluntary motor control at the PMd level.

4 Materials and methods

4.1 Subjects

Two male rhesus macaque monkeys (Macaca mulatta, Monkeys P and C), weighing 9 and 9.5 kg, respectively, were used. Animal care, housing, surgical procedures and experiments conformed to European (Directive 86/609/ECC and 2010/63/UE) and Italian (D.L. 116/92 and D.L. 26/2014) laws and were approved by the Italian Ministry of Health. Monkeys were pair-housed with cage enrichment. They were fed daily with standard primate chow that was supplemented with nuts and fresh fruits if necessary. During recording days, the monkeys received their daily water supply during the experiments.

4.2 Apparatus and task

The monkeys were seated in front of a black isoluminant background ($< 0.1cd/m2$) of a 17-inch touchscreen monitor (LCD, 800 x 600 resolution), inside a darkened, acoustic-insulated room. A non-commercial software package, CORTEX (http://www.nimh.gov.it), was used to control the presentation of the stimuli and the behavioural responses. Fig.1 shows the scheme of the general task: a stop-signal reaching task[24]. Each trial started with the appearance of a central target (CT) (red circle, diameter 1.9 cm). The monkeys had to reach and hold the CT. After a variable holding time (400–900 ms, 100 ms increments) a peripheral target (PT) (red circle, diameter 1.9 cm) appeared randomly in one of two possible locations (right/left) and the CT disappeared (Go signal). In Go trials, after the Go signal the subjects had to reach and hold the PT for a variable time (400-800 ms, 100 ms increments) to receive juice. Reaction times (RTs) were defined as the time between the presentation of the Go signal and the onset of the hand movement. In Stop trials, the sequence of events was the same until the Go signal. Then, after a variable delay (Stop signal delay SSD), the CT reappeared (Stop signal) and the monkeys had to hold the CT until the end of the trial, (800–1000 ms) to receive the reward (correct Stop trial). Conversely, removing the hand after the Stop signal constituted a wrong response (wrong Stop trial). The same amount of juice was delivered for correct Stop and correct Go trials. The inter-trial interval was set to 800 ms. Stop trials represented on average the 25% of all trials for Monkey P and 32% for Monkey C. White circles around the central target were used as feedback for the animals to indicate the touch. To establish the duration of the SSDs, a staircase tracking procedure was employed. If the monkey succeeded in withholding the response, the SSD increased by one step (100 ms) in the subsequent Stop signal trial. Conversely, if the subject failed, the SSD decreased by one step.

4.3 Behavioural considerations

The stop-signal reaching task makes possible to calculate a behavioural measure that is broadly considered as an index of efficiency in movement suppression: the Stop signal reaction time or SSRT. To estimate the SSRT the race model[94] is the accepted paradigm. This model describes the behaviour in the Stop trials as the result of two stochastic processes racing toward a threshold: the GO process triggered by the onset of the Go signal, which duration is represented by the RT, and the STOP process triggered by the onset of the Stop signal, which duration must be calculated. When the GO process wins the race the movement is generated (wrong Stop trials), alternatively, it is withheld (correct Stop trials). The race model allows us to estimate the SSRT by considering the duration of the GO process, the probability of response and the SSDs. However, to make the race model applicable to study response inhibition, a central assumption must be satisfied: the GO process in the Stop trials must be the same as in the Go trials (independence assumption). Indeed, the RTs that are employed to estimate the SSRT are obtained

from the Go trials distributions. To broadly validate this assumption, wrong Stop trials RTs must result shorter than the correct Go trials RTs[94] (see Table 1). To estimate the SSRT we employed the integration method because it has been proven to be the most reliable[95]. The method assumes that the finishing time of the Stop process corresponds to the *n*th Go RT, where *n* results from the multiplication of the ordered Go RTs distribution by the overall probability of responding $p(respond)$. The SSRT is then obtained by subtracting the average SSD from the *n*th Go RT. The SSRT can also be considered as the lead time that is required to inhibit a movement, or, simply, the time that precedes the start of a movement when a Stop signal, if presented, halts the generation of the same movement approximately 50% of the time. If the Stop signal is presented after this time, it will be less effective, because the neuronal phenomena that lead to movement generation will have already been started. If the Stop signal is presented before this time, it will be more effective in halting the movement. Consequently, the neuronal activity that is related to movement generation must occur before movement onset around the time that is defined by the SSRT. The aim of our study was to compare conditions in which a movement was planned and then generated (Go trials) to those in which a movement was planned and then inhibited (correct Stop trials). To correctly compare the two behavioural conditions, a time window (T) equivalent for both trial types must be defined. The duration of T corresponded to 400 ms. For Go trials, T was the last portion of the RT. For Stop trials, T allowed to include any SSRT duration computed in the different sessions (see Table 1) and a variable portion of the SSD (controlling for the duration of the shortest used). Behavioural parameters for the recording sessions of the two monkeys analyzed in this study are reported in Table 1.

4.4 Extraction and processing of neuronal data

A multielectrode array (Blackrock Microsystems, Salt Lake City) with 96 electrodes (spacing 0.4 mm) was surgically implanted in the left dorsal premotor cortex (PMd; arcuate sulcus and pre-central dimple used as references after the opening of the dura) to acquire unfiltered electric field potentials (UFP; i.e., the raw signal) sampled at 24.4 kHz (Tucker Davis Technologies, Alachua, FL). As a measure of neuronal activity at the population level, local spiking activity (SA) was extracted offline from the raw signal, as in Mattia et al.[7], by computing the time-varying power spectra $P(\omega, t)$ from the short-time Fourier transform of the signal in 5-ms sliding windows. Relative spectra $R(\omega, t)$ were then obtained normalizing $P(\omega, t)$ by their average $P_{ref}(\omega)$ across a fixed window (30 minutes) for the entire recording. Thus, the average $R(\omega, t)$ across the $\omega/2\pi$ band $[0.2, 1.5]\ kHz$ represent the spectral estimated spiking activity (SA). As better detailed in Mattia et al.[7], such an estimate relies on two hypotheses. The first is that high ω components of the raw signal result from the convolution of firing rates $\nu(t)$ of neurons that are close to the electrode tip with a stereotypical single-unit waveform. The Fourier transform $K(\omega)$ of such an unknown waveform is canceled out in $R(\omega, t)$, which is therefore a good approximation of the ratio of firing rate spectra $|\nu(\omega,t)|^2 / |\nu(\omega,t)|_{ref}{}^2$. The second hypothesis is that high ω power $|\nu(\omega,t)|^2$ is proportional to the firing rate $\nu(t)$ itself[96], such that our estimated spiking activity is proportional to $\nu(t)$. As a last step, logarithmically scaled SAs were smoothed by a moving average (40 ms sliding window, 5ms step).

4.5 Quantifying information dynamics with Transfer Entropy

To examine the local information dynamics in the PMd we used multivariate Transfer Entropy[97,98] (*TE*). The choice is due to the fact that TE is indicated, especially in its multivariate formulations, as more accurate compared to other metrics and is known to capture non-linear interaction in the system dynamic without assuming any particular model. Moreover, this measure is of growing interest in neuroscience and there is a thriving literature on it[51,99–104]. Given an ensemble of M time series, the multivariate information transfer from a *driver* time series X to a *target* time series Y, conditioned to the remaining $Z_{k=1,..,M-2}$ time series, can be quantified considering the present values of the target and the past values

of both the driver and the Z through[99,105,106]:

$$TE_{X\to Y\,|\,Z} = H(Y_n \mid Y_n^-, Z_n^-) - H(Y_n \mid Y_n^-, X_n^-, Z_n^-)\ , \tag{1}$$

where Y_n is the vector that represent the present state n of Y, $X_n^- = [X_{n-1}, X_{n-2}, ...]$, $Y_n^- = [Y_{n-1}, Y_{n-2}, ...]$ and $Z_n^- = [Z_{n-1}, Z_{n-2}, ...]$ are the vectors that represent the past of X, Y and Z respectively. The vertical bar stands for conditional probability, e.g. $H(Y_n \mid Y_n^-, Z_n^-)$ is the entropy of the present state of Y conditioned to the knowledge of the past of Y and to the past of the remaining Z. H is the Shannon entropy[107], which in the case of Y is given by:

$$H(Y_n) = -\sum_n P(Y_n)\, log P(Y_n)\ , \tag{2}$$

where P indicates the probability density. Hence, using equation 2 expression 1 becomes

$$TE_{X\to Y\,|\,Z} = -\sum_n P(Y_n, Y_n^-, X_n^-, Z_n^-)\, log \frac{P(Y_n \mid Y_n^-, X_n^-, Z_n^-)}{P(Y_n \mid Y_n^-, Z_n^-)} \tag{3}$$

TE is by definition ≥ 0 and in this formulation *TE* grows if the past of the driver increases the information about the present of target more than the past of target itself and more than any other series contained in Z. Since the past of the driver is used to predict the present of the target, TE is not symmetric (i.e. $TE_{X\to Y} \neq TE_{Y\to X}$) and defines a direction in the information transfer. A crucial issue when estimating TE is the approximation of the vectors representing the past of the time series, a procedure known as *embedding*. The optimal embedding would be the one that includes only the components of X_n^-, Y_n^- and Z_n^- that are most informative in describing Y_n. Montalto and colleagues described in detail different procedures both for embedding and evaluating the probability distribution functions needed to compute the entropy terms[105]. We opted for a non-uniform embedding scheme[108] paired with the computation of H based on kernels estimators[1]. In few words, the embedding method we chose iteratively selects components of the systems past based on a criterion for maximum relevance and minimum redundancy. In this context, maximum relevance means most significant in the sense of predictive information. Non-uniform embedding selects from the past of X, Y and Z only the components that are the most informative for the present of the target variable Y, progressively pruning non informative terms. The maximum number of past values, or maximum lag l, to consider for the pruning is fixed at the beginning of the procedure. The statistical significance is then progressively assessed cycling through the components of the past (up to l) and through the comparison with an null distribution built from the empirical values via a randomization procedure[105]. The components of the past of X,Y and Z are thus selected as statistical significant if they are significant above a desired level α. In our case the null distribution was obtained by 300 random shuffling of empirical values and we fixed $\alpha = 0.01$. Non-uniform embedding represents a convenient and more reliable[99] alternative to the common used approach known as uniform embedding. This would indeed select the past values X_n^-, Y_n^- and Z_n^- *a priori* and separately for each time series[105]. The probability densities needed for the computations of H were calculated using the Kernel estimator. The Kernel estimator reconstructs the probability distribution at each data point by using kernel functions which weight the distance from the reference point to any other point in the time series. Such approach

[1]For the complete description of the embedding methods and estimators for computation of H, which is beyond the scope of this study, see the works of Faes and colleagues and references therein[106,108,109].

exploits a local exploring of the state space which make it more robust against unreliable estimations compared to other approaches[99]. Therefore, if at least one component from the past is selected by the non-uniform embedding procedure, the resulting $TE_{X \to Y \mid Z}$ is > 0 and statistically significant. When instead none of the components of the past provide statically significant information about the target the $TE_{X \to Y \mid Z} = 0$ and assumed non significant[105]. To avoid any further bias in the selection of the past values we initially fixed a very "distant" l=50 ms, but, as expected, only a recent past was selected by the procedure, in line with similar studies[41,47,51]. Indeed, for each SA time series, a past no older than 10ms for each n of equation 2 was ever selected by the optimal embedding procedure. This was very much expected since it is known that neuronal populations in the cortex are likely to create causal interaction and exchange information in a temporal range from 1 to 20 ms[110,111]. Within this framework, we then built the single-trial information transfer networks, for each behavioural condition of each recording session, by adapting some functions of the Matlab *MUTE* toolbox[105] to our data-analysis pipeline. Since the use of information theory techniques in neuroscience is still a developing field, it is worth making some brief general remarks on the application of such techniques on invasive neurophysiological data. For a technical discussion see the work of Gomez-Herrero[112], Bossomaier[104], Wibral[101] and colleagues. For a specific and comprehensive discussion of all the critical points in the field, refer to Timme and Lapish's seminal review[113]. As summarized perfectly in the latter, the fundamental assumption made by the experimenters in applying information theory tools to neural data concerns the stationarity of the neural processes under investigation. Stationarity of a process means that the probability density function generating the observable variables do not change over time. This involves assuming that each observation contributes to the same probability distribution. In operational terms, this translates into treating the experimental trials as multiple realizations of the same underlying process. In other words, assuming stationarity implies that each observed realization (i.e., the experimental trials) contributes to delineating the same underlying probability distribution[51] which, eventually, remains stable over time (i.e., the duration of the experiment). Thus, in the case of a behavioral neurophysiology experiment, the observations correspond to the values of neural activity, the realizations to the repeated trials and the probability distribution to the probability distribution characteristic of the investigated neural process which is supposed to generate the observed behaviour. It is of absolute importance to remember that in any experimental paradigm this distribution is not known *a priori* and is almost never accessible. This is a fundamental difference from any theoretical study, in which time series are generated based on many realizations of processes whose analytical details are known. Moreover, as discussed by Wollstadt and coworkers[51], it is also worth stressing that stationarity does not imply a flat variability over the realizations. Some variance it is instead expected, as it reflects the natural variance of the underlying (unknown) probability distribution. For these reasons, when an experiment has a multi-trial structure, stationarity over realizations is assumed valid by default, provided that no slow drifts or trends are present in the signal. The presence of trends in the time series is indeed one of the non-stationarity factors that can affect a correct estimation of TE[99]. In a behavioral neurophysiology experiment, these could arise during training or in an experiment that facilitates learning[51]. In fact, these are the most common situations in which the probability distribution of both the neural signal and the behavioral parameters change, by definition, over time. As a first step in using TE on our data, we analysed the single-trials SA profiles of each module for each recording session for both animals. Our estimate of SAs is baseline corrected (see section 4.4) thus eliminating any possible distorting slow trends. Moreover, to remove noisy outliers from our data, we excluded from the analysis the trials for which the SAs showed peaks with an amplitude that exceeded the average of the activity by 2 standard deviations in any of the time bins of the epoch of interest and for over 80% of the channels[15] (< 2% of the total number of trials). This ensures that artifacts caused by non-physiological peaks and/or segments of oscillations of high variance in the time series are excluded from the analysis. As explained

in detail by Xiong and coworkers[99], these kinds of non-stationary artifacts are among those that most impinge on a reliable estimation of TE. Indeed, if present, they would affect the probability distributions in equation 3 in such a way that most of the signal variance would be dominated by outliers. As a result, the estimation of the temporal relationship between the present and the past states of the time series would be substantially biased. To this regard, as described above, the kernel estimator is particularly helpful since it manages to remove any potential residual dependence of the estimated TE on the variance of the signal thanks to the finer local exploring of the state space.

4.6 Graph theoretical analysis

In our context the time series were the local SAs recorded by the electrodes of the array. We computed $TE_{X \to Y \mid Z}$ (and $TE_{Y \to X \mid Z}$) with $Z_{k=1,..,M-2}$, for each pair of (X,Y) in the T epoch defined in Section 4.3 so to obtain a single-trial TE matrix for each behavioural condition (Go trials, correct and wrong Stop trials) for both monkeys. We interpreted the TE matrix as the adjacency matrix of a directed weighted network in which the nodes are the single modules (electrodes) and the weighted edges are the $TE_{X \to Y \mid Z}$ (and $TE_{Y \to X \mid Z}$) with $Z_{k=1,..,M-2}$. To simplify the picture we ignored the main diagonal of the matrix thus excluding self-loops from the networks. Finding an optimal threshold to analyze network properties is a major challenge when dealing with connectivity matrices. To overcome the hindrance we used percolation, as we did in our previous works[15,30]. Percolation is a method that is rooted in statistical physics and, since its first applications to the study of phase transitions of connected subgraphs in random networks[114], has progressively entered the toolbox of those neuroscientists interested in the hierarchical organization of brain networks[31–33,37–39,115–117]. During percolation the stability of network topology is monitored via the iterative removal of links based on the value of their weights. Therefore, the process naturally discloses both network robustness properties and signatures of hierarchical self-organization simultaneously. This straightforwardly exposes the details of the complexity of network arrangement. Moreover, recent studies have shown that percolation leads to the robust identification of a specific network threshold that achieves the best balance between the removal of noise-induces spurious links and the consequent loss of information potentially encoded in those links[31,33]. In the present work we used percolation for this purpose. At the beginning of our analysis pipeline, we implemented percolation on the trial-averaged TE network to prune the weaker links affected by the the inevitable statistical noise introduced by the operation of averaging over trials. In this regard, it is informative to discuss two aspects of the issue. The first concerns the use of our version of percolation analysis as a fine-grained cleaning tool for spurious values of TE. Indeed, in practical situations, it is legitimate to expect some "leaks" of non-zero TE measurements even when there is no such a directed relationship between the variables[104]. This is due to the finite (and often small) number of samples available to the experimenter. Introducing percolation analysis into our pipeline, as a second check after the bias-corrected estimators described in Section 4.5, easily solves this problem in a topology-based and completely data-driven fashion. The second regards the averaging over trials. Simulation studies have reported that for stationary data (or for those that are at least to a first approximation, as in the case of multi-trial structured neural data) the averaging operation leads to satisfactory results even in the case of relatively short time series[102]. As an alternative, a set of powerful methods, called ensemble methods, have been proposed. These methods exploit the multi-trials structure to improve the temporal resolution of the TE estimation[51,102,112]. Intuitively, the operation of averaging over trials can be thought of as a "vertical" operation in which TE is estimated from single-trial time series and then averaged over trials in a fixed time window. In contrast, ensemble methods perform a more "horizontal" operation by estimating TE for each time point by exploiting the

ensemble of neural activity values across all trials[2]. In this study, we opted for the former method. Indeed, we were interested in describing the state of the PMd information network at a specific epoch of the task and comparing it across experimental conditions. To do so, we needed multiple realizations of the network so that we could extract a robust average representation and a reliable statistic for its topological measures. Instead, an ensemble method would have inevitably led to a single, albeit temporally accurate, realization of the network for each behavioral condition[51,101]. Since the networks analyzed here are weighted and directed, it was necessary to apply the percolation analysis on the giant strongly connected component of the networks, and not on the connected component as usually done in the case of undirected graphs[118,119]. Very briefly, a directed graph is strongly connected if every vertex is reachable from every other vertex following the direction of the links. Therefore, given an arbitrary directed graph a strongly connected component is a subgraph that is strongly connected. Beyond its use as an effective thresholding method, percolation was employed in this work to characterize the overall topology of the network in the three behavioral conditions and to investigate how the hierarchical interactions between classes shaped the level of complexity of such configurations. Percolation analysis yields a curve which shows the size of the largest connected component as a function of link weights. Therefore, link weights represent the thresholds used to monitor the network disintegration. The power of percolation discloses when the curve exhibits a stepped pattern, meaning that the network fragments progressively under the removal of links. Thus, each step in the curve entails the presence of a transient stable configuration of the network, made of hierarchical interaction between nodes. Conversely, in the case of links arranged with a higher degree of randomness, a steeper curve with no (or very few) jumps is found, which implies a single incipient connected component dominating the network and rapidly fragmenting in a single step. In addition, the threshold at which the fragmentation of the largest component begins, gives indications about the complexity of the network. In the present work, such a threshold, which is formally called the percolation threshold, has been referred to for simplicity as the "descent point" of the curves A fragmentation at higher thresholds (i.e., for higher link values) signals a component with many of its nodes sharing their strongest links within the component. This implies a more complex arrangement of connections and, consequently, communications that tend to be directed more inwards within the component itself than outwards. We then used the percolation threshold to measure the level of network complexity during the different behavioral conditions. Please refer to the work of Gallos and colleagues and to our previous works for more formal details of the percolation analysis applied to brain networks[15,30,37]. To inspect the contribution of the hubs we measured the Vertex Degree (VD). VD is the number of links to a node i:

$$VD_{\mathrm{i}} = \sum_{j=1}^{N} a_{\mathrm{ij}} \ , \tag{4}$$

where a_{ij} is the generic entry of the adjacency matrix and N is the number of nodes. In directed networks one can distinguish between in-degree (the number on inward links) and out-degree (the number of outward links). We computed the probability distribution of both VDs (i.e. the in/out degree distribution) for each behavioural condition of each recording sessions for both animals. If the variance of the degree distribution is significantly larger than its mean, tails in the distribution arise and network hubs are identified (see Figure S1). Therefore, hubs are nodes that significantly exceed the average degree of the network (here we used mean $\pm$ 2 standard deviations of the out-degree distributions)[34,35]. Once hubs were identified, to further skim their contribution to the information exchange in the network we grouped

[2]Even a brief technical *excursus* on this family of methods would require too much space in this context, so we limit ourselves to this brief simile to get the main point.

them according to the behavioural condition in which they emerged. We labeled the hubs according to the two possible outcomes of the motor behaviours explored in the task, i.e. movement generation (Go trials) and movement inhibition (correct Stop trials). In more details, if a node is a hub in Go trials but not in correct Stop trials, it belongs to the Go_drivers. Vice versa it belongs to the Stop_drivers. If a node is a hub in both conditions it belongs to the Super_drivers. The hybrid situation, i.e. wrong Stop trials, was then used as a benchmark for the labeling procedure: if different hubs were present in the wrong Stop trials than those found in Go and correct Stop trials, they would appear in Fig.4, Fig.6, S2, S3 and S4 as high VD nodes whose links would have a "new" color. Since this does not happen, we infer that the only hubs are those identified using Go and correct Stop trials and that there is no specific class of "wrong Stop_drivers." This selection procedure identified the classes. In our framework, the TE values represented the strength of the connections between nodes and hence the classes are defined based on how much and during which behavioural condition nodes spread information within the local PMd network. Successively, to summarize in one number the total magnitude of information exchanged between the classes we constructed the following interaction measure I:

$$I_{\mathrm{ij}}{}^{(\mathrm{m,n})} = \rho \sum_{i}^{M} \sum_{j}^{M} \sum_{(m,n)} TE_{C_{\mathrm{i}}{}^{\mathrm{m}} \rightarrow C_{\mathrm{j}}{}^{\mathrm{n}}} \,, \tag{5}$$

where C is the module's class, M is the number of classes (M=4) and m and n run over the all possible combinations of nodes within each class. $\rho = \frac{1}{dim\,(C_{\mathrm{i}})}$ is a normalization factor that accounts for the heterogeneous number of nodes within each of the classes. Therefore, our $\mathrm{I_{ij}}$ is a normalized node strength computed on the graph formed by the 4 classes (i.e. in a weighted graph the strength of a node is the sum of the weights of the links connected to the node). Hence, the values and the directions of I reflect the position in the hierarchy of the network communications for that class. All the interactions described by the empirical TE matrix were thus enclosed in a 4x4 matrix that represented a network of interactions in which now each node is a functional class. We computed I for each recording session and each behavioural condition and then obtained the sessions-averaged (mean $\pm$ SEM) element $\bar{I}_{\mathrm{ij}}$ (Figure 8 and supplementary Table S3 and S4) for both animals.

4.6.1 A node-based multifractal analysis: NMFA

We used the node-based multifractal analysis (NMFA), recently proposed by Xiao and colleagues[40], to reveal the generating rules of the PMd information network and expose its fractal features across behavioral conditions. This robust and reliable mathematical framework provides a way to formally quantify the fractal properties of a network, thereby capturing the multi-scale details of its topology. NMFA discloses the high-order connectivity patterns and link them with the intrinsic functionalities of the network, providing, at the same time, a general criterion by which the structural distance between networks can be efficiently measured. For a formal discussion of fractal analysis methods in the context of complex network theory, which is beyond the scope of this paper, please refer to the references cited below, to the work by Xiao and colleagues[40] and the references therein. The NMFA approach is inspired by an algorithm traditionally used to quantify the fractal properties of complex networks: the box-covering method[120,121]. In the box-covering algorithm the fractal properties are measured through the minimum number of subgraphs (the boxes) of size l (in the sense of network distance) required to cover the whole network. The fractality of the network is then quantified by the number l^{-D_f}, in which D_f is the fractal dimension. This number describes well the self-similarity properties of the system when the network structure is not particularly inhomogeneous. Inhomogeneities are present, for example, when a network

exhibits fluctuations in the local density of nodes. This is the case for networks that have hubs[36,122]. This is a specific example of a more general criterion that states that any inhomogeneous distribution of a physical parameter on a fractal object frequently shows multifractal features[123]. This is the reason why the traditional methods[124,125], such the box-covering, falls short of capturing the structural scaling dependence in some real networks, which restricts its applicability. Thus, since the properties of a multifractal system differ from the "position" one has within the system (in the case of a network, from what node one is considering), D_f alone is no longer enough. Instead, a spectrum of measurements is needed, called the multifractal spectrum, which weights the fractal properties of the system according to the inhomogeneities in it[126]. NMFA extends the box-covering algorithm so that it accounts for multifractality by introducing a parameter q, called distortion exponent, that weights the fractal features of each node in a probabilistic manner[123,127]. By slightly modifying the notation of Xiao and colleagues, we define the probability $u_i(r)$ associated with the node i as $u_i(r) = \frac{N_i(r)}{N}$, where r is the radius of the growing box (the analogous of the aforementioned l). $u_i(r)$ weights the inhomogeneities in the network by measuring how much the neighborhood of node i is crowded. In the NMFA approach, r is varied from 0, that corresponds to a box centered on the node i and containing i only, until it covers the entire network. $N_i(r)$ is the number of nodes contained in the box of size r and N is the total number of nodes in the network. Let us now define $U_q(r)$ as the sum of the qth power of $u_i(r)$. $U_q(r)$ is a relevant quantity, called partition function, and gives fundamental statistical insights on the system under investigation. $U_q(r)$ is defined as:

$$U_q(r) = \sum_{1}^{N} u_i(r)^q. \tag{6}$$

When q>0, frequent network motifs are taken into account in the weighting procedure. When q<0, rare network motifs count more. Calling D the diameter of the network, which also corresponds to the maximum radius r for the growing box, one can observe that $U_q(r) \sim (\frac{r}{d})^{\tau(q)}$ where $\tau(q)$ is called the mass exponent. $\tau(q)$ is calculated as

$$\tau(q) = \frac{ln(U_q(r))}{ln(\frac{r}{d})}. \tag{7}$$

We can then introduce the generalized fractal dimension[126] $D(q)$ as

$$D(q) = \frac{\tau(q)}{q} \tag{8}$$

and the multifractal spectrum $F(\alpha)$ as

$$F(\alpha) = q\alpha(q) - \tau(q), \tag{9}$$

where $\alpha(q) = \frac{d\tau(q)}{dq}$ is the Lipschiz–Holder exponent. $D(q)$ quantifies the dimension of the fractal features of the network and $F(\alpha)$ explicitly shows how such features are distributed as a function of the Lipschiz–Holder exponent α. $D(q)$ and $F(\alpha)$ are mathematically related: $F(\alpha)$ is the Legendre transform of $D(q)$. Through $D(q)$ and $F(\alpha)$, powerful metrics regarding the complexity and heterogeneity of the topology of a network can be obtained. One is the Asymmetry metric that is defined as:

$$Asymmetry = ln(\frac{\alpha_0 - \alpha_{min}}{\alpha_{max} - \alpha_0}). \tag{10}$$

where α_0 is the abscissa corresponding to the maximum of $F(\alpha)$, α_{max} and α_{min} are the maximum and minimum values taken by α respectively. The values of α_0 give detailed information about the structural organization of a network and can distinguish even small changes in its topology: $\alpha_0 \approx 1$ indicate a regular topology while $\alpha_0 \approx 3$ a topology characterized by an increasing degree of randomness which consequently raise the degree of heterogeneity and complexity of the network. The Asymmetry metric is closely related to the shape of the multifractal spectrum $F(\alpha)$ in the following way: a network with a topology endowed with hubs has a spectrum with tails toward the left and Asymmetry > 0; a purely random network has a spectrum with tails toward the right and Asymmetry < 0. Values of Asymmetry ≈ 0 indicate a topology with no real dominant structure. Another metric, d, can be derived that quantifies the structural distance between two networks. Since $D(q)$ quantifies the multifractal properties of the network, d between network 1 and 2 can be defined as:

$$d = \sqrt{\frac{\int_{q_{min}}^{q_{max}} (D_1(q) - D_2(q))^2 dq}{q_{max} - q_{min}}}. \tag{11}$$

d determines how much the topological structures of the two networks differ.

4.6.2 A null model

To further assess the statistical significance of the results, beyond what was already done by the randomization procedure included in the TE computations, we defined a null network model. As extensively detailed in a recent work[128], the choice of a suitable null model remains a thorny issue in network and complex systems science. One common practice when analysing real-world networks, such the ones inspected in the present work, is try to identify properties that deviate from the null hypothesis, being likely that the deviations themselves encode information about the network functions. In this study, we drew our conclusions about the PMd information network in a completely data-driven fashion, directly from neural activity, which thus constituted our only constraint. Therefore, we tested whether the results were not attributable to the distribution of SA values and the dimensions of the corresponding time series. However, in the latter case our sample size was safely far from the limits of reliability reported in the literature for comparable systems[103, 113], but we still used it in the null model as an additional control. We generated, for each trial of each behavioural condition and recording session, a synthetic pool of N time series with same length of the empirical ones (with N number of recording channels) by random sampling from the empirical SA distribution. We then computed the trial-averaged TE matrix for each synthetic pool. This situation is the most general since assumptions of any kind are made on the connectivity patterns and the weight distributions of the synthetic networks. We then compared the set of our empirical measures with those obtained from the ensemble of 500 randomizations. As widely expected, the degree distributions of the experimental networks had a variance at least one order of magnitude higher than that of the networks derived from the SA distribution despite having comparable mean values (see supplementary figure S5).

Acknowledgements

Partially supported by grants from Sapienza University (PH11715C823A9528 to SF and RM11916B89232364 to PP), from EC FP7 grant 'BrainLeap' (to SF), from grant 'Borse di Studio 2020' Fondazione Baroni (to GB), and from EC ERANET CHIST-ERA 2019 grant 'MUCCA' (to SF).

Author contributions statement

F.G, P.P., E.B. and S.F conceived the experiment, F.G. and P.P. conducted the experiment, G.B. and V.G. analysed the results. All authors reviewed the manuscript.

Data availability statement

Data are available from the corresponding author upon reasonable request.

Competing interests

The authors report no declarations of interest.

References

1. Hong, G. & Lieber, C. M. Novel electrode technologies for neural recordings. *Nat. Rev. Neurosci.* **20**, 330–345, 10.1038/s41583-019-0140-6 (2019).

2. Ferraina, S., Paré, M. & Wurtz, R. H. Comparison of cortico-cortical and cortico-collicular signals for the generation of saccadic eye movements. *J. Neurophysiol.* **87**, 845–858, 10.1152/jn.00317.2001 (2002).

3. Wurtz, R. H., Sommer, M. A., Paré, M. & Ferraina, S. Signal transformations from cerebral cortex to superior colliculus for the generation of saccades. *Vis. Res.* **41**, 3399–3412, 10.1016/S0042-6989(01)00066-9 (2001).

4. Herreras, O. Local Field Potentials: Myths and Misunderstandings. *Front. Neural Circuits* **10**, 101, 10.3389/fncir.2016.00101 (2016).

5. Stark, E. & Abeles, M. Predicting movement from multiunit activity. *J. Neurosci.* **27**, 8387–8394, 10.1523/JNEUROSCI.1321-07.2007 (2007).

6. Trautmann, E. M. *et al.* Accurate Estimation of Neural Population Dynamics without Spike Sorting. *Neuron* **103**, 292–308, 10.1016/j.neuron.2019.05.003 (2019).

7. Mattia, M. *et al.* Heterogeneous attractor cell assemblies for motor planning in premotor cortex. *J. Neurosci.* **33**, 11155–11168, 10.1523/JNEUROSCI.4664-12.2013 (2013).

8. Riehle, A., Grün, S., Diesmann, M. & Aertsen, A. Spike synchronization and rate modulation differentially involved in motor cortical function. *Science* **278**, 1950–1953, 10.1126/science.278.5345.1950 (1997).

9. Georgopoulos, A. P., Schwartz, A. B. & Kettner, R. E. Neuronal population coding of movement direction. *Science* **233**, 1416–1419, 10.1126/science.3749885 (1986).

10. Munoz, D. P. & Wurtz, R. H. Fixation cells in monkey superior colliculus I. Characteristics of cell discharge. *J. Neurophysiol.* **70**, 559–575, 10.1152/jn.1993.70.2.559 (1993).

11. Schall, J. D. Visuomotor Functions in the Frontal Lobe. *Annu. Rev. Vis. Sci.* **1**, 469–498, 10.1146/annurev-vision-082114-035317 (2015).

12. Vaadia, E., Kurata, K. & Wise, S. P. Neuronal activity preceding directional and nondirectional cues in the premotor cortex of rhesus monkeys. *Somatosens. & Mot. Res.* **6**, 207–230, 10.3109/08990228809144674 (1988).

13. Fetz, E. E. Are movement parameters recognizably coded in the activity of single neurons? *Behav. Brain Sci.* **15**, 679–690, 10.1017/S0140525X00072599 (1992).

14. Vyas, S., Golub, M. D., Sussillo, D. & Shenoy, K. V. Computation through Neural Population Dynamics. *Annu. Rev. Neurosci.* **43**, 249–275, 10.1146/annurev-neuro-092619-094115 (2020).

15. Bardella, G., Pani, P., Brunamonti, E., Giarrocco, F. & Ferraina, S. The small scale functional topology of movement control: Hierarchical organization of local activity anticipates movement generation in the premotor cortex of primates. *NeuroImage* **207**, 10.1016/j.neuroimage.2019.116354 (2020).

16. Giarrocco, F. *et al.* Neuronal dynamics of signal selective motor plan cancellation in the macaque dorsal premotor cortex. *Cortex* **135**, 326–340, 10.1016/j.cortex.2020.09.032 (2021).

17. Hubel, D. H. & Wiesel, T. N. Receptive fields, binocular interaction and functional architecture in the cat's visual cortex. *The J. Physiol.* **160**, 106–154, 10.1113/jphysiol.1962.sp006837 (1962).

18. Wise, S. P., Boussaoud, D., Johnson, P. B. & Caminiti, R. Premotor and parietal cortex: Corticocortical connectivity and combinatorial computations. *Annu. Rev. Neurosci.* **20**, 25–42, 10.1146/annurev.neuro.20.1.25 (1997).

19. Cisek, P. & Kalaska, J. F. Neural mechanisms for interacting with a world full of action choices. *Annu. Rev. Neurosci.* **33**, 269–298, 10.1146/annurev.neuro.051508.135409 (2010).

20. Shenoy, K. V., Sahani, M. & Churchland, M. M. Cortical Control of Arm Movements: A Dynamical Systems Perspective. *Annu. Rev. Neurosci.* **36**, 337–359, 10.1146/annurev-neuro-062111-150509 (2013).

21. Milekovic, T., Truccolo, W., Grün, S., Riehle, A. & Brochier, T. Local field potentials in primate motor cortex encode grasp kinetic parameters. *NeuroImage* **114**, 338–355, 10.1016/J.NEUROIMAGE.2015.04.008 (2015).

22. Georgopoulos, A. P., Kalaska, J. F., Caminiti, R. & Massey, J. T. On the relations between the direction of two-dimensional arm movements and cell discharge in primate motor cortex. *The J. neuroscience : official journal Soc. for Neurosci.* **2**, 1527–1537, 10.1523/JNEUROSCI.02-11-01527.1982 (1982).

23. Caminiti, R., Johnson, P. B., Galli, C., Ferraina, S. & Burnod, Y. Making arm movements within different parts of space: the premotor and motor cortical representation of a coordinate system for reaching to visual targets. *J. Neurosci.* **11**, 1182–1197, 10.1523/JNEUROSCI.11-05-01182.1991 (1991).

24. Mirabella, G., Pani, P. & Ferraina, S. Neural correlates of cognitive control of reaching movements in the dorsal premotor cortex of rhesus monkeys. *J. Neurophysiol.* **106**, 1454–1466, 10.1152/jn.00995.2010 (2011).

25. Ramawat, S. *et al.* Different Contribution of the Monkey Prefrontal and Premotor Dorsal Cortex in Decision Making During a Transitive Inference Task. *Neuroscience* **485**, 147–162, 10.1016/J.NEUROSCIENCE.2022.01.013 (2022).

26. Pani, P. *et al.* Visual salience of the stop signal affects the neuronal dynamics of controlled inhibition. *Sci. Reports 2018 8:1* **8**, 1–13, 10.1038/s41598-018-32669-8 (2018).

27. Battaglia-Mayer, A. *et al.* Correction and suppression of reaching movements in the cerebral cortex: Physiological and neuropsychological aspects, 10.1016/j.neubiorev.2014.03.002 (2014).

28. Pani, P. *et al.* Alpha- and beta-band oscillations subserve different processes in reactive control of limb movements. *Front. behavioral neuroscience* **8**, 10.3389/FNBEH.2014.00383 (2014).

29. Pani, P. *et al.* Neuronal population dynamics during motor plan cancellation in nonhuman primates. *Proc. Natl. Acad. Sci. United States Am.* **119**, e2122395119, 10.1073/pnas.2122395119 (2022).

30. Bardella, G., Bifone, A., Gabrielli, A., Gozzi, A. & Squartini, T. Hierarchical organization of functional connectivity in the mouse brain: A complex network approach. *Sci. Reports* **6**, 1–11, 10.1038/srep32060 (2016).

31. Bordier, C., Nicolini, C. & Bifone, A. Graph analysis and modularity of brain functional connectivity networks: Searching for the optimal threshold. *Front. Neurosci.* **11**, 441, 10.3389/fnins.2017.00441 (2017).

32. Nicolini, C. & Bifone, A. Modular structure of brain functional networks: breaking the resolution limit by Surprise. *Sci. Reports* **6**, 10.1038/SREP19250 (2016).

33. Nicolini, C., Bordier, C. & Bifone, A. Community detection in weighted brain connectivity networks beyond the resolution limit. *NeuroImage* **146**, 28–39, 10.1016/j.neuroimage.2016.11.026 (2017).

34. Albert, R. & Barabási, A.-L. Statistical mechanics of complex networks. *Rev. Mod. Phys.* **74**, 47–97, 10.1103/RevModPhys.74.47 (2002).

35. Barabási, A. L. Network science, 10.1098/rsta.2012.0375 (2013).

36. Barabási, A. L. & Albert, R. Emergence of scaling in random networks. *Science* **286**, 509–512, 10.1126/science.286.5439.509 (1999).

37. Gallos, L. K., Makse, H. A. & Sigman, M. A small world of weak ties provides optimal global integration of self-similar modules in functional brain networks. *Proc. Natl. Acad. Sci. United States Am.* **109**, 2825–2830, 10.1073/pnas.1106612109 (2012).

38. Mastrandrea, R. *et al.* Organization and hierarchy of the human functional brain network lead to a chain-like core. *Sci. Reports 2017 7:1* **7**, 1–13, 10.1038/s41598-017-04716-3 (2017).

39. Mastrandrea, R. *et al.* The unbalanced reorganization of weaker functional connections induces the altered brain network topology in schizophrenia. *Sci. Reports* **11**, 15400, 10.1038/S41598-021-94825-X (2021).

40. Xiao, X., Chen, H. & Bogdan, P. Deciphering the generating rules and functionalities of complex networks. *Sci. Reports 2021 11:1* **11**, 1–15, 10.1038/s41598-021-02203-4 (2021).

41. Shimono, M. & Beggs, J. M. Functional clusters, hubs, and communities in the cortical microconnectome. *Cereb. Cortex* **25**, 3743–3757, 10.1093/cercor/bhu252 (2015).

42. Buehlmann, A. & Deco, G. Optimal information transfer in the cortex through synchronization. *PLoS Comput. Biol.* **6**, 1000934, 10.1371/journal.pcbi.1000934 (2010).

43. Orlandi, J. G., Stetter, O., Soriano, J., Geisel, T. & Battaglia, D. Transfer entropy reconstruction and labeling of neuronal connections from simulated calcium imaging. *PLoS ONE* **9**, 98842, 10.1371/journal.pone.0098842 (2014).

44. Thivierge, J.-P. Scale-free and economical features of functional connectivity in neuronal networks. *PHYSICAL REVIEW E* **90**, 22721, 10.1103/PhysRevE.90.022721 (2014).

45. Ito, S. *et al.* Extending Transfer Entropy Improves Identification of Effective Connectivity in a Spiking Cortical Network Model. *PLoS ONE* **6**, e27431, 10.1371/journal.pone.0027431 (2011).

46. Nigam, S. *et al.* Rich-club organization in effective connectivity among cortical neurons. *J. Neurosci.* **36**, 655–669, 10.1523/JNEUROSCI.2177-15.2016 (2016).

47. Timme, N. M. *et al.* High-Degree Neurons Feed Cortical Computations. *PLOS Comput. Biol.* **12**, e1004858, 10.1371/journal.pcbi.1004858 (2016).

48. Gerhard, F., Pipa, G., Lima, B., Neuenschwander, S. & Gerstner, W. Extraction of Network Topology From Multi-Electrode Recordings: Is there a Small-World Effect? *Front. Comput. Neurosci.* **5**, 4, 10.3389/fncom.2011.00004 (2011).

49. Besserve, M., Lowe, S. C., Logothetis, N. K., Schölkopf, B. & Panzeri, S. Shifts of Gamma Phase across Primary Visual Cortical Sites Reflect Dynamic Stimulus-Modulated Information Transfer. *PLoS Biol.* **13**, e1002257, 10.1371/journal.pbio.1002257 (2015).

50. Honey, C. J., Kötter, R., Breakspear, M. & Sporns, O. Network structure of cerebral cortex shapes functional connectivity on multiple time scales. *Proc. Natl. Acad. Sci. United States Am.* **104**, 10240–10245, 10.1073/pnas.0701519104 (2007).

51. Wollstadt, P., Martínez-Zarzuela, M., Vicente, R., Díaz-Pernas, F. J. & Wibral, M. Efficient transfer entropy analysis of non-stationary neural time series. *PLoS ONE* **9**, 102833, 10.1371/journal.pone.0102833 (2014).

52. Jahfari, S. *et al.* Effective connectivity reveals important roles for both the hyperdirect (fronto-subthalamic) and the indirect (fronto-striatal-pallidal) fronto-basal ganglia pathways during response inhibition. *J. Neurosci.* **31**, 6891–6899, 10.1523/JNEUROSCI.5253-10.2011 (2011).

53. Boucher, L., Palmeri, T. J., Logan, G. D. & Schall, J. D. Inhibitory control in mind and brain: An interactive race model of countermanding saccades. *Psychol. Rev.* **114**, 376–397, 10.1037/0033-295X.114.2.376 (2007).

54. Lo, C. C., Boucher, L., Paré, M., Schall, J. D. & Wang, X. J. Proactive inhibitory control and attractor dynamics in countermanding action: A spiking neural circuit model. *J. Neurosci.* **29**, 9059–9071, 10.1523/JNEUROSCI.6164-08.2009 (2009).

55. Gupta, G., Pequito, S. & Bogdan, P. Dealing with Unknown Unknowns: Identification and Selection of Minimal Sensing for Fractional Dynamics with Unknown Inputs. *2018 Annu. Am. Control. Conf. (ACC)* **2018-June**, 2814–2820, 10.23919/ACC.2018.8430866 (2018).

56. Suárez, L. E., Markello, R. D., Betzel, R. F. & Misic, B. Linking Structure and Function in Macroscale Brain Networks. *Trends Cogn. Sci.* **24**, 302–315, 10.1016/J.TICS.2020.01.008 (2020).

57. Xue, Y. & Bogdan, P. Reconstructing missing complex networks against adversarial interventions. *Nat. Commun. 2019 10:1* **10**, 1–12, 10.1038/s41467-019-09774-x (2019).

58. Yang, R., Sala, F. & Bogdan, P. Hidden network generating rules from partially observed complex networks. *Commun. Phys. 2021 4:1* **4**, 1–12, 10.1038/s42005-021-00701-5 (2021).

59. Churchland, M. M. *et al.* Neural population dynamics during reaching. *Nature* **487**, 51–56, 10.1038/nature11129 (2012).

60. Chandrasekaran, C., Peixoto, D., Newsome, W. T. & Shenoy, K. V. Laminar differences in decision-related neural activity in dorsal premotor cortex. *Nat. Commun.* **8**, 1–16, 10.1038/s41467-017-00715-0 (2017).

61. Kaufman, M. T. *et al.* The largest response component in the motor cortex reflects movement timing but not movement type. *eNeuro* **3**, 85–101, 10.1523/ENEURO.0085-16.2016 (2016).

62. Clawson, W. *et al.* Computing hubs in the hippocampus and cortex. *Sci. Adv.* **5**, eaax4843, 10.1126/sciadv.aax4843 (2019).

63. Schroeder, K. E. *et al.* Disruption of corticocortical information transfer during ketamine anesthesia in the primate brain. *NeuroImage* **134**, 459–465, 10.1016/j.neuroimage.2016.04.039 (2016).

64. Marcos, E. *et al.* Neural variability in premotor cortex is modulated by trial history and predicts behavioral performance. *Neuron* **78**, 249–255, 10.1016/j.neuron.2013.02.006 (2013).

65. Verbruggen, F. & Logan, G. D. Response inhibition in the stop-signal paradigm, 10.1016/j.tics.2008.07.005 (2008).

66. Schall, J. D., Palmeri, T. J. & Logan, G. D. Models of inhibitory control. *Philos. Transactions Royal Soc. B: Biol. Sci.* **372**, 20160193, 10.1098/rstb.2016.0193 (2017).

67. Wei, W., Rubin, J. E. & Wang, X. J. Role of the indirect pathway of the basal ganglia in perceptual decision making. *J. Neurosci.* **35**, 4052–4064, 10.1523/JNEUROSCI.3611-14.2015 (2015).

68. Drummond, N. M., Cressman, E. K. & Carlsen, A. N. Go-activation endures following the presentation of a stop-signal: evidence from startle. *J Neurophysiol* **117**, 403–411, 10.1152/jn.00567.2016.-It (2017).

69. Dunovan, K., Lynch, B., Molesworth, T. & Verstynen, T. Competing basal ganglia pathways determine the difference between stopping and deciding not to go. *eLife* **4**, 10.7554/ELIFE.08723 (2015).

70. Gu, Y., Qi, Y. & Gong, P. Rich-club connectivity, diverse population coupling, and dynamical activity patterns emerging from local cortical circuits. *PLoS Comput. Biol.* **15**, e1006902, 10.1371/journal.pcbi.1006902 (2019).

71. Perin, R., Berger, T. K. & Markram, H. A synaptic organizing principle for cortical neuronal groups. *Proc. Natl. Acad. Sci. United States Am.* **108**, 5419–5424, 10.1073/pnas.1016051108 (2011).

72. Timme, N. *et al.* Multiplex Networks of Cortical and Hippocampal Neurons Revealed at Different Timescales. *PLoS ONE* **9**, e115764, 10.1371/journal.pone.0115764 (2014).

73. Schroeter, M. S., Charlesworth, P., Kitzbichler, M. G., Paulsen, O. & Bullmore, E. T. Emergence of rich-club topology and coordinated dynamics in development of hippocampal functional networks In vitro. *J. Neurosci.* **35**, 5459–5470, 10.1523/JNEUROSCI.4259-14.2015 (2015).

74. Gal, E. *et al.* Rich cell-type-specific network topology in neocortical microcircuitry. *Nat. Neurosci.* **20**, 1004–1013, 10.1038/nn.4576 (2017).

75. Dann, B., Michaels, J. A., Schaffelhofer, S. & Scherberger, H. Uniting functional network topology and oscillations in the fronto-parietal single unit network of behaving primates. *eLife* **5**, 10.7554/eLife.15719 (2016).

76. Hilgetag, C., O'Neill, M. A. & Young, M. P. Hierarchical organization of macaque and cat cortical sensory systems explored with a novel network processor. *Philos. Transactions Royal Soc. London. Ser. B: Biol. Sci.* **355**, 71–89, 10.1098/rstb.2000.0550 (2000).

77. Hilgetag, C. C. & Kaiser, M. Clustered organization of cortical connectivity, 10.1385/NI:2:3:353 (2004).

78. Felleman, D. J. & Van Essen, D. C. Distributed Hierarchical Processing in the Primate Cerebral Cortex. *Cereb. Cortex* **1**, 1–47, 10.1093/CERCOR/1.1.1-A (1991).

79. Sporns, O., Tononi, G. & Kötter, R. The Human Connectome: A Structural Description of the Human Brain. *PLoS Comput. Biol.* **1**, e42, 10.1371/journal.pcbi.0010042 (2005).

80. Kaiser, M. Hierarchy and dynamics of neural networks. *Front. Neuroinformatics* **4**, 112, 10.3389/fninf.2010.00112 (2010).

81. Zamora-López. Cortical hubs form a module for multisensory integration on top of the hierarchy of cortical networks. *Front. Neuroinformatics* **4**, 1, 10.3389/neuro.11.001.2010 (2010).

82. Zeki, S. & Shipp, S. The functional logic of cortical connections. *Nature* **335**, 311–317, 10.1038/335311a0 (1988).

83. Tononi, G., Sporns, O. & Edelman, G. M. A measure for brain complexity: Relating functional segregation and integration in the nervous system. *Proc. Natl. Acad. Sci. United States Am.* **91**, 5033–5037, 10.1073/pnas.91.11.5033 (1994).

84. Sporns, O., Honey, C. J. & Kötter, R. Identification and Classification of Hubs in Brain Networks. *PLoS ONE* **2**, e1049, 10.1371/journal.pone.0001049 (2007).

85. Watanabe, T. *et al.* Energy landscapes of resting-state brain networks. *Front. Neuroinformatics* **8**, 12, 10.3389/fninf.2014.00012 (2014).

86. Kaiser, M., Görner, M. & Hilgetag, C. C. Criticality of spreading dynamics in hierarchical cluster networks without inhibition. *New J. Phys.* **9**, 110, 10.1088/1367-2630/9/5/110 (2007).

87. Hilgetag, C. C. & Goulas, A. 'Hierarchy' in the organization of brain networks. *Philos. Transactions Royal Soc. B: Biol. Sci.* **375**, 20190319, 10.1098/rstb.2019.0319 (2020).

88. Fox, M. D. *et al.* The human brain is intrinsically organized into dynamic, anticorrelated functional networks. *Proc. Natl. Acad. Sci. United States Am.* **102**, 9673–9678, 10.1073/pnas.0504136102 (2005).

89. He, B. J. Scale-free properties of the functional magnetic resonance imaging signal during rest and task. *J. Neurosci.* **31**, 13786–13795, 10.1523/JNEUROSCI.2111-11.2011 (2011).

90. Zalesky, A., Fornito, A., Cocchi, L., Gollo, L. L. & Breakspear, M. Time-resolved resting-state brain networks. *Proc. Natl. Acad. Sci. United States Am.* **111**, 10341–10346, 10.1073/pnas.1400181111 (2014).

91. Shine, J. M. *et al.* The Dynamics of Functional Brain Networks: Integrated Network States during Cognitive Task Performance. *Neuron* **92**, 544–554, 10.1016/j.neuron.2016.09.018 (2016).

92. Vidaurre, D., Smith, S. M. & Woolrich, M. W. Brain network dynamics are hierarchically organized in time. *Proc. Natl. Acad. Sci. United States Am.* **114**, 12827–12832, 10.1073/pnas.1705120114 (2017).

93. Morcos, A. S. & Harvey, C. D. History-dependent variability in population dynamics during evidence accumulation in cortex. *Nat. Neurosci.* **19**, 1672–1681, 10.1038/nn.4403 (2016).

94. Logan, G. D. & Cowan, W. B. On the ability to inhibit thought and action: A theory of an act of control. *Psychol. Rev.* **91**, 295–327, 10.1037//0033-295x.91.3.295 (1984).

95. Band, G. P., van der Molen, M. W. & Logan, G. D. Horse-race model simulations of the stop-signal procedure. *Acta Psychol.* **112**, 105–142, 10.1016/S0001-6918(02)00079-3 (2003).

96. Mattia, M. & Del Giudice, P. Population dynamics of interacting spiking neurons. *Phys. Rev. E - Stat. Physics, Plasmas, Fluids, Relat. Interdiscip. Top.* **66**, 19, 10.1103/PhysRevE.66.051917 (2002).

97. Schreiber, T. Measuring information transfer. *Phys. Rev. Lett.* **85**, 461–464, 10.1103/PhysRevLett.85.461 (2000).

98. Komárek, V., Hrnčíř, Z. & Štěrbová, K. Synchronization as adjustment of information rates: Detection from bivariate time series. *Phys. Rev. E* **63**, 046211, 10.1103/PhysRevE.63.046211 (2001).

99. Xiong, W., Faes, L. & Ivanov, P. C. Entropy measures, entropy estimators, and their performance in quantifying complex dynamics: Effects of artifacts, nonstationarity, and long-range correlations. *Phys. Rev. E* **95**, 1–37, 10.1103/PhysRevE.95.062114 (2017).

100. Vicente, R., Wibral, M., Lindner, M. & Pipa, G. Transfer entropy-a model-free measure of effective connectivity for the neurosciences. *J. Comput. Neurosci.* **30**, 45–67, 10.1007/s10827-010-0262-3 (2011).

101. Wibral, M. *et al.* Transfer entropy in magnetoencephalographic data: Quantifying information flow in cortical and cerebellar networks. *Prog. Biophys. Mol. Biol.* **105**, 80–97, 10.1016/j.pbiomolbio.2010.11.006 (2011).

102. Michael Wibral, J. T. L., Raul Vicente (ed.) *Directed Information Measures in Neuroscience | SpringerLink* (Springer Berlin, Heidelberg, 2014), 1 edn.

103. Ramos, A. M. T., Macau, E. E. N., Lopes, A. M. & Machado, J. A. T. Minimum Sample Size for Reliable Causal Inference Using Transfer Entropy. *Entropy 2017* **19**, 150, 10.3390/E19040150 (2017).

104. Bossomaier, T., Barnett, L., Harré, M. & Lizier, J. T. *An introduction to transfer entropy: Information flow in complex systems* (Springer International Publishing, 2016).

105. Montalto, A., Faes, L. & Marinazzo, D. MuTE: A MATLAB toolbox to compare established and novel estimators of the multivariate transfer entropy. *PLoS ONE* **9**, e109462, 10.1371/journal.pone.0109462 (2014).

106. Faes, L., Kugiumtzis, D., Nollo, G., Jurysta, F. & Marinazzo, D. Estimating the decomposition of predictive information in multivariate systems. *PHYSICAL REVIEW E* **91**, 32904, 10.1103/PhysRevE.91.032904 (2015).

107. Shannon, C. E. A Mathematical Theory of Communication. *The Bell Syst. Tech. J.* **27**, 623–656 (1948).

108. Faes, L., Marinazzo, D., Montalto, A. & Nollo, G. Lag-specific transfer entropy as a tool to assess cardiovascular and cardiorespiratory information transfer. *IEEE Transactions on Biomed. Eng.* **61**, 2556–2568, 10.1109/TBME.2014.2323131 (2014).

109. Faes, L., Nollo, G. & Porta, A. Information-based detection of nonlinear Granger causality in multivariate processes via a nonuniform embedding technique. *Phys. Rev. E - Stat. Nonlinear, Soft Matter Phys.* **83**, 051112, 10.1103/PhysRevE.83.051112 (2011).

110. Mason, A., Nicoli, A. & Stratford, K. Synaptic transmission between individual pyramidal neurons of the rat visual cortex in vitro. *J. Neurosci.* **11**, 72–84, 10.1523/JNEUROSCI.11-01-00072.1991 (1991).

111. Swadlow, H. A. Efferent neurons and suspected interneurons in motor cortex of the awake rabbit: axonal properties, sensory receptive fields, and subthreshold synaptic inputs. *J. neurophysiology* **71**, 437–453, 10.1152/JN.1994.71.2.437 (1994).

112. Gómez-Herrero, G. *et al.* Assessing Coupling Dynamics from an Ensemble of Time Series. *Entropy 2015, Vol. 17, Pages 1958-1970* **17**, 1958–1970, 10.3390/E17041958 (2015).

113. Timme, N. M. & Lapish, C. A Tutorial for Information Theory in Neuroscience. *eNeuro* **5**, 10.1523/ENEURO.0052-18.2018 (2018).

114. Callaway, D. S., Newman, M. E., Strogatz, S. H. & Watts, D. J. Network Robustness and Fragility: Percolation on Random Graphs. *Phys. Rev. Lett.* **85**, 5468, 10.1103/PhysRevLett.85.5468 (2000).

115. Vlasov, V. & Bifone, A. Hub-driven remote synchronization in brain networks. *Sci. Reports 2017 7:1* **7**, 1–11, 10.1038/s41598-017-09887-7 (2017).

116. Bordier, C., Nicolini, C., Forcellini, G. & Bifone, A. Disrupted modular organization of primary sensory brain areas in schizophrenia. *NeuroImage: Clin.* **18**, 682–693, 10.1016/j.nicl.2018.02.035 (2018).

117. Del Ferraro, G. *et al.* Finding influential nodes for integration in brain networks using optimal percolation theory. *Nat. Commun. 2018 9:1* **9**, 1–12, 10.1038/s41467-018-04718-3 (2018).

118. Graf, A. On the Strongly Connected Components of Random Directed Graphs with Given Degree Sequences. Tech. Rep., University of Waterloo (2016).

119. Squires, S. *et al.* Weakly explosive percolation in directed networks. *PHYSICAL REVIEW E* **87**, 52127, 10.1103/PhysRevE.87.052127 (2013).

120. Song, C., Havlin, S. & Makse, H. A. Self-similarity of complex networks. *Nat. 2005 433:7024* **433**, 392–395, 10.1038/nature03248 (2005).

121. Song, C., Gallos, L. K., Havlin, S. & Makse, H. A. How to calculate the fractal dimension of a complex network: The box covering algorithm. *J. Stat. Mech. Theory Exp.* 10.1088/1742-5468/2007/03/P03006 (2007).

122. Furuya, S. & Yakubo, K. Multifractality of complex networks. *Phys. Rev. E - Stat. Nonlinear, Soft Matter Phys.* **84**, 036118, 10.1103/PHYSREVE.84.036118/FIGURES/2/MEDIUM (2011).

123. Paladin, G. & Vulpiani, A. Anomalous scaling laws in multifractal objects. *Phys. Reports* **156**, 147–225, 10.1016/0370-1573(87)90110-4 (1987).

124. Rendón De La Torre, S., Kalda, J., Kitt, R. & Engelbrecht, J. THE EUROPEAN PHYSICAL JOURNAL B Fractal and multifractal analysis of complex networks: Estonian network of payments. *Eur. Phys. J. B* **90**, 234, 10.1140/epjb/e2017-80214-5 (2017).

125. Alonso, L., Méndez-Bermúdez, J. A. & Estrada, E. Geometrical and spectral study of β-skeleton graphs. *Phys. Rev. E* **100**, 062309, 10.1103/PHYSREVE.100.062309/FIGURES/13/MEDIUM (2019).

126. Cencini, M., Cecconi, F. & Vulpiani, A. *Chaos: From Simple Models to Complex Systems* (World Scientific Publishing Co., 2009).

127. Grassberger, P., Badii, R. & Politi, A. Scaling Laws for Invariant Measures on Hyperbolic and Nonhyperbolic Atractors. *J. Stat. Phys.* **51** (1988).

128. Cimini, G. *et al.* The statistical physics of real-world networks. *Nat. Rev. Phys.* **1**, 58–71, 10.1038/s42254-018-0002-6 (2019).